arXiv:1407.1932v1 [physics.plasm-ph] 8 Jul 2014

Fourier–Hermite spectral representation for the Vlasov–Poisson system in the weakly collisional limit

J. T. PARKER[1]† **AND P. J. DELLAR**[1]

[1] Mathematical Institute, University of Oxford, Andrew Wiles Building, Radcliffe Observatory Quarter, Woodstock Road, Oxford, U.K., OX2 6GG

(Received ?; revised ?; accepted ?. - To be entered by editorial office)

We study Landau damping in the 1+1D Vlasov–Poisson system using a Fourier–Hermite spectral representation. We describe the propagation of free energy in phase space using forwards and backwards propagating Hermite modes recently developed for gyrokinetics [Schekochihin et al. (2014)]. The change in the electric field corresponds to the net Hermite flux via a free energy evolution equation. In linear Landau damping, decay in the electric field corresponds to forward propagating Hermite modes; in nonlinear damping, the initial decay is followed by a growth phase characterised by the generation of backwards propagating Hermite modes by the nonlinear term. The free energy content of the backwards propagating modes increases exponentially until balancing that of the forward propagating modes. Thereafter there is no systematic net Hermite flux, so the electric field cannot decay and the nonlinearity effectively suppresses Landau damping. These simulations are performed using the fully-spectral 5D gyrokinetics code SpectroGK [Parker et al. 2014], modified to solve the 1+1D Vlasov–Poisson system. This captures Landau damping via an iterated Lénard–Bernstein collision operator or via Hou–Li filtering in velocity space. Therefore the code is applicable even in regimes where phase-mixing and filamentation are dominant.

PACS codes: Authors should not enter PACS codes directly on the manuscript, as these must be chosen during the online submission process and will then be added during the typesetting process (see http://www.aip.org/pacs/ for the full list of PACS codes)

1. Introduction

Many phenomena in astrophysical and fusion plasmas require a kinetic rather than a fluid description. The fundamental quantity is the distribution function $F(\boldsymbol{x}, \boldsymbol{v}, t)$ that determines the number density of particles at position $\boldsymbol{x}$ moving with velocity $\boldsymbol{v}$ at time t. Numerical computations of the evolution of the distribution function in its six-dimensional phase space are thus very demanding on resources. Even simulations using the reduced five-dimensional gyrokinetic formulation (e.g. Howes *et al.* 2006; Krommes 2012) are restricted to modest resolutions in each dimension. For example, simulations by Highcock *et al.* (2011) with the gyrokinetic code `GS2` (Dorland *et al.* 2009) used $64 \times 32 \times 14$ points in physical space, and the equivalent of 24×16 points in velocity space. This has motivated the development of our fully spectral gyrokinetic code SpectroGK (Parker *et al.* 2014). A fully spectral representation of the distribution function may

† Email address for correspondence: parkerj@maths.ox.ac.uk

be expected to make optimal use of the limited number of degrees of freedom possible in each dimension. Moreover, we have established that the spectral representation in SpectroGK correctly captures Landau damping in a reduced linear problem for ion temperature gradient driven instabilities (Parker & Dellar 2014).

The Vlassov–Poisson and Vlassov–Poisson–Fokker–Planck systems are canonical mathematical models for kinetic phenomena in plasmas (*e.g.* Glassey 1996). They describe a single active species moving in a fixed background charge distribution, which we take to be uniform with unit density for convenience:

$$\partial_t F + \mathbf{v} \cdot \nabla_{\mathbf{x}} F - \mathbf{E} \cdot \nabla_{\mathbf{v}} F = \nu C[F], \tag{1.1a}$$

$$\mathbf{E} = -\nabla \Phi, \tag{1.1b}$$

$$-\nabla^2 \Phi = 1 - \int_{-\infty}^{\infty} \mathrm{d}\mathbf{v}\ F. \tag{1.1c}$$

Here $\nabla_{\mathbf{x}}$ and $\nabla_{\mathbf{v}}$ denote gradients with respect to $\mathbf{x}$ and $\mathbf{v}$, $\mathbf{E}$ is the electric field derived from the electrostatic potential Φ. The right-hand side of the Poisson equation (1.1*c*) contains the uniform background charge, and the charge due to the particles described by F. Physically, this system describes electron-scale Langmuir turbulence in which the much more massive ions remain immobile. The right-hand side of (1.1*c*) represents particle collisions with rate ν using a Fokker–Planck operator $C[F]$ as described below.

The collisionless ($\nu = 0$) linearised 1+1 dimensional form of the Vlasov–Poisson system is a canonical mathematical model for the "filamentation" or "phase-mixing" that forms infinitesimally fine scale structures in velocity space due to the shearing effect of the particle streaming term $\mathbf{v} \cdot \nabla_{\mathbf{x}} F$. Landau (1946) showed that this system supports solutions in which the potential Φ decays exponentially in time (see also Balescu 1963; Lifshitz & Pitaevskii 1981). Landau obtained this solution via a Laplace transform in time, and a deformation of the contour in the integral (1.1*c*) defining Φ to ensure its analytic continuity. The distribution function F does not itself decay in time, but instead develops ever finer scales. The Landau-damping solution is thus not an eigenfunction of the collisionless system. Instead, the system has a continuous spectrum of real eigenvalues associated with non-decaying singular eigenfunctions called Case–Van Kampen modes (Van Kampen 1955; Case 1959). The Case–Van Kampen modes are complete, so the Landau-damped solution may be expressed as an infinite superposition of them.

Lénard & Bernstein (1958) showed that the velocity-space diffusion due to a Fokker–Planck collision term $\nu C[F]$ with any strictly positive frequency $\nu > 0$ creates a smooth eigenfunction whose frequency and damping rate approached those of the electric field in Landau's solution as $\nu \to 0$. Ng *et al.* (1999, 2004) showed that the collisionally regularised system in fact has a discrete spectrum of smooth eigenfunctions that form a complete set. A subset of these eigenfunctions have eigenvalues that tend to solutions of Landau's dispersion relation (see section 4.1) in the limit of vanishing collisions (Ng *et al.* 2006). As $\nu \to 0$, the smooth eigenfunctions develop boundary layers with widths proportional to the decay rates $|\gamma|$ of the modes, in which F oscillates with a wavelength proportional to $\nu^{-1/4}$ (Ng *et al.* 2006).

Any strictly positive collision frequency $\nu > 0$ thus suffices to change the spectrum of the integro-differential equation from continuous to discrete. However, for numerical computations it is necessary to make the velocity space discrete, either through introducing a grid, or through representing F as a finite sum of orthogonal functions (see below). Either approach introduces a finest resolved scale in the velocity space. The transition from collisional to collisionless behaviour then occurs at some finite collision frequency ν^*, for which the oscillations in the eigenfunctions are just coarse enough to be resolved

(Parker & Dellar 2014). This critical frequency ν^* is resolution-dependent, and tends to zero in the limit of infinite resolution. When $\nu < \nu^*$, the system's behaviour is "collisionless": all eigenfunctions decay more slowly than the Landau rate. When $\nu = 0$ the eigenfunctions are discrete Case–Van Kampen modes with real eigenvalues, and hence no decay. One cannot obtain a discrete analogue of the Landau-damped solution from a linear combination of this finite set of eigenfunctions.

Only when $\nu \geqslant \nu^*$ do we find a decaying eigenmode in the discretised system that is resolved, and whose decay rate approximates the Landau rate. Since $\nu^* \to 0$ as resolution increases, the decay rate of the slowest decaying resolved mode tends to the Landau rate with increasing velocity space resolution. We have found that very accurate approximations to the Landau rate can be achieved with a very modest number, around 10, degrees of freedom in velocity space by using an iterated Lénard–Bernstein collision operator (Parker & Dellar 2014).

The above discussion applies to linearised 1+1 dimensional kinetic theory. The question of how to capture Landau damping numerically also arises in the much more complex nonlinear and multi-dimensional simulations of astrophysical and fusion plasmas, for which the canonical model is the five-dimensional "gyrokinetic" system (see reviews by Howes *et al.* 2006; Krommes 2012). Charged particles in magnetic fields spiral around the field lines. When the magnetic field is sufficiently strong, the fast timescales and short lengthscales of this "gyromotion" may be eliminated by averaging over the particle gyrations. This averaging also reduces the dimensionality of phase space from 6 to 5, with velocity space components parallel and perpendicular to the magnetic field.

A linearized 1+1 dimensional electrostatic version of gyrokinetics for motions parallel to the magnetic field is obtained by integrating out the velocity dependence perpendicular to the magnetic field (as before) and taking the limit of vanishing perpendicular wavenumber. The perturbation f of the ion distribution function $\tilde{f} = f + f_0$ relative to a Maxwellian f_0 then evolves according to the gyrokinetic system

$$\frac{\partial f}{\partial t} + v\frac{\partial f}{\partial z} = E\frac{\partial f_0}{\partial v}, \tag{1.2a}$$

$$E = -\frac{\partial \Phi}{\partial z}, \tag{1.2b}$$

$$\Phi = \int_{-\infty}^{\infty} \mathrm{d}v \; f, \tag{1.2c}$$

where z and v are the physical space and velocity space coordinates parallel to the magnetic field. The previous Poisson equation (1.1c) has been replaced by the quasineutrality condition (1.2c). This condition holds at lengthscales much larger than the Debye length, and on slow ion timescales for which the electrons may be assumed to adopt an instantaneous Maxwell–Boltzmann distribution proportional to $\exp(\Phi/(k_B T_e))$. The system (1.2a-c) is otherwise identical to the perturbative form of the Vlasov–Poisson system derived in section 2.

The availability of high quality numerical solutions to the 1+1 dimensional Vlasov–Poisson system makes it a good benchmark for novel numerical algorithms. Due to the high dimensionality, gyrokinetic simulations can typically only afford relatively coarse resolution in each dimension. Our fully spectral gyrokinetic code SpectroGK uses a spectral representation in each dimension to make optimal use of a limited number of degrees of freedom. The 1+1 dimensional version of SpectroGK reduces to a Fourier–Hermite representation with spectral filtering, or hypercollisions, to provide dissipation at the smallest resolved scales in z and v.

Burnett (1935, 1936) expanded the distribution function as a sum of spherical har-

monics multiplying polynomials that are orthogonal with respect to the Gaussian weight function that appears in the Maxwell–Boltzmann equilibrium distribution. The Hermite polynomials have this orthogonality property in one dimension (Abramowitz & Stegun 1972) so Grad (1949*a*,*b*, 1958) introduced sets of tensor Hermite polynomials as a Cartesian alternative to Burnett's expansion. Both expansions conveniently convert an integro-differential kinetic equation into an infinite hierarchy of partial differential equations for the expansion coefficients.

The same expansion in Hermite polynomials for velocity space, and in Fourier modes for physical space, was used in early simulations of the 1+1 dimensional Vlasov–Poisson system, such as by Armstrong (1967), Grant & Feix (1967) and Joyce *et al.* (1971), albeit with different forms of dissipation and, inevitably, much lower resolution than is currently feasible.

However, as higher dimensional models became computationally feasible, interest turned instead to particle-in-cell (PIC) methods. These represent the distribution function using a set of macro-particles located at discrete points $(\boldsymbol{x}_i, \boldsymbol{v}_i)$ in phase space, each of which represents many physical ions or electrons (Dawson 1983; Hockney & Eastwood 1988; Birdsall & Langdon 2004). The method exploits the structure of the left-hand side of the kinetic equation (1.1*a*) as a derivative along a characteristic in phase space. A PIC method evolves the solution by propagating macro-particles along their characteristics, analogous to the Lagrangian formulation of fluid dynamics. The representation of the continuous function $F(\boldsymbol{x}, \boldsymbol{v}, t)$ by a discrete set of n macro-particles creates an $O(1/\sqrt{n})$ sampling error, sometimes called "shot noise", that creates particular difficulties in the tail of the distribution where F is much smaller than its maximum value.

More recent multi-dimensional gyrokinetics codes have returned to Eulerian representations of velocity space, using fixed grids either for parallel velocities (Jenko *et al.* 2000; Peeters *et al.* 2009) or for pitch angles (Fahey & Candy 2004; Dorland *et al.* 2009). However Hermite polynomials have been used to develop reduced kinetic (Zocco & Schekochihin 2011) and gyrofluid models (Hammett *et al.* 1993; Parker & Carati 1995), as well as the Hermite index being used as a quantity of interest in characterizing velocity space behaviour (Schekochihin *et al.* 2014; Kanekar *et al.* 2014; Plunk & Parker 2014). This has reignited interest in using Hermite polynomials for computation in new reduced-dimension (Hatch *et al.* 2013; Loureiro *et al.* 2013) gyrokinetics codes, and the fully five-dimensional SpectroGK.

In this paper we illustrate the solution of the Vlasov–Poisson system with the Fourier–Hermite method using a modified version of the SpectroGK gyrokinetics code. We demonstrate that both hypercollisionality (*e.g.* Joyce *et al.* 1971) and a velocity space form of the Hou & Li (2007) spectral filter suffice to prevent recurrence and result in correct calculations even in regimes where filementation and Landau damping are dominant.

We derive the one-dimensional system in section 2 and the Fourier–Hermite spectral representation in section 3, before testing the implementation by studying nonlinear Landau damping and the two stream instability in section 4.

2. The 1+1-dimensional Vlasov–Poisson system

We derive a 1+1-dimensional form of the Vlasov–Poisson system (1.1a-c) by seeking solutions which have spatial dependence in the z direction only, and integrating over the velocity components $\boldsymbol{v}_\perp$ perpendicular to the z direction. The reduced distribution

function $\tilde{f}(z,v,t) = \int \mathrm{d}^2\boldsymbol{v}_\perp\ F(\boldsymbol{x},\boldsymbol{v},t)$ obeys the system

$$\frac{\partial \tilde{f}}{\partial t} + v\frac{\partial \tilde{f}}{\partial z} - E\frac{\partial \tilde{f}}{\partial v} = \nu C[\tilde{f}], \tag{2.1}$$

$$E = -\frac{\partial \Phi}{\partial z}, \tag{2.2}$$

$$-\frac{\partial^2 \Phi}{\partial z^2} = 1 - \int_{-\infty}^{\infty} \mathrm{d}v\ \tilde{f}, \tag{2.3}$$

where v and E are the components of $\boldsymbol{v}$ and $\boldsymbol{E}$ in the z direction. We take the domain of the problem to be $(z,v) \in \Omega \times \mathbb{R}$ where $\Omega = [0,L]$, and consider periodic boundary conditions for $\tilde{f}$ in space, while in velocity space $\tilde{f}(z,v,t) \to 0$ as $|v| \to \infty$. Overall charge neutrality requires that the integral of (2.3) over Ω vanishes, so that $E = -\partial\Phi/\partial z$ is periodic on Ω. A detailed discussion of other boundary conditions may be found in Heath *et al.* (2012).

It is useful to consider the decomposition $\tilde{f} = f_0 + f$ where $f_0(v)$ is a stationary, spatially-uniform distribution function satisfying

$$1 = \int_{-\infty}^{\infty} \mathrm{d}v\ f_0. \tag{2.4}$$

Equations (2.1)–(2.3) then become

$$\frac{\partial f}{\partial t} + v\frac{\partial f}{\partial z} - E\frac{\partial f}{\partial v} = E\frac{\partial f_0}{\partial v}, \tag{2.5}$$

$$E = -\frac{\partial \Phi}{\partial z}, \tag{2.6}$$

$$\frac{\partial^2 \Phi}{\partial z^2} = \int_{-\infty}^{\infty} \mathrm{d}v\ f, \tag{2.7}$$

and the overall charge neutrality condition becomes

$$\int_\Omega \mathrm{d}z \int_{-\infty}^{\infty} \mathrm{d}v\ f(z,v,t) = 0. \tag{2.8}$$

Equation (2.5) implies that this condition holds for all subsequent times, provided it holds initially. The decomposed system (2.5)–(2.7) holds for any decomposition satisfying (2.4), but it is particularly useful for small perturbations about an equilibrium, for when $|f| \ll |f_0|$ and $|\partial f/\partial v| \ll |\partial f_0/\partial v|$, the linearized system may be readily obtained by neglecting the single nonlinear term $-E\partial f/\partial v$ in (2.5).

For comparison, the corresponding linear 1+1 dimensional form of the gyrokinetic equations originally targetted by SpectroGK is

$$\frac{\partial f}{\partial t} + v\frac{\partial f}{\partial z} = E\frac{\partial f_0}{\partial v}, \tag{2.9a}$$

$$E = -\frac{\partial \Phi}{\partial z}, \tag{2.9b}$$

$$\Phi = \int_{-\infty}^{\infty} \mathrm{d}v\ f. \tag{2.9c}$$

The nonlinear term in (2.5) does not appear even in the nonlinear gyrokinetic system under the standard ordering that assumes lengthscales in z, oriented along the background magnetic field, are much larger than lengthscales in the perpendicular directions.

The dissipationless Vlasov–Poisson system (2.1)–(2.3) with $\nu = 0$ conserves the total

momentum P and energy H given by

$$P = \int_\Omega \mathrm{d}z \int_{-\infty}^{\infty} \mathrm{d}v \; v\tilde{f}(z,v,t), \tag{2.10}$$

$$H = \frac{1}{2}\int_\Omega \mathrm{d}z \int \mathrm{d}v \; v^2\tilde{f}(z,v,t) + \frac{1}{2}\int_\Omega \mathrm{d}z \; |E(z,t)|^2. \tag{2.11}$$

It also conserves a family of Casimir invariants

$$C = \int_\Omega \mathrm{d}z \int_{-\infty}^{\infty} \mathrm{d}v \; \mathcal{C}(\tilde{f}), \tag{2.12}$$

where $\mathcal{C}(\tilde{f})$ is any function of $\tilde{f}$ alone. For example, taking $\mathcal{C}(\tilde{f}) = \tilde{f}$ shows that the system conserves the total particle number

$$N = \int_\Omega \mathrm{d}z \int_{-\infty}^{\infty} \mathrm{d}v \; \tilde{f}(z,v,t). \tag{2.13}$$

This ensures that the time evolution preserves the overall neutrality condition (2.8). Another conserved quantity of this form is the the spatially-integrated Boltzmann entropy

$$\mathcal{H}[\tilde{f}] = \int_\Omega \mathrm{d}z \; \int_{-\infty}^{\infty} \mathrm{d}v \; \tilde{f}\log\tilde{f}, \tag{2.14}$$

for which $\mathcal{C}(\tilde{f}) = \tilde{f}\log\tilde{f}$.

In conjuction with the decomposition $\tilde{f} = f_0 + f$ it is useful to consider the spatially-integrated relative entropy (*e.g.* Bardos *et al.* 1993; Pauli 2000)

$$\mathcal{R}[\tilde{f}|f_0] = \int_\Omega \mathrm{d}z \; \int_{-\infty}^{\infty} \mathrm{d}v \; \tilde{f}\log\left(\frac{\tilde{f}}{f_0}\right) - \tilde{f} + f_0. \tag{2.15}$$

This quantity has been employed to establish rigorous hydrodynamic limits of the Boltzmann equation (Lions & Masmoudi 2001; Golse & Saint-Raymond 2004), to establish the existence and long-time attractive properties of steady solutions of the Vlasov–Poisson system (Bouchut 1993; Dolbeault 1999) and for other plasma applications (Krommes & Hu 1994; Hallatschek 2004). Expanding (2.15) for small perturbations $f = \tilde{f} - f_0 \ll f_0$ gives

$$\mathcal{R}[\tilde{f}|f_0] = \int_\Omega \mathrm{d}z \; \int_{-\infty}^{\infty} \mathrm{d}v \; \frac{f^2}{2f_0} + O\left(f^3\right), \tag{2.16}$$

so the relative entropy provides a sign-definite quadratic measure of small perturbations from a uniform state.

However, the relative entropy is not itself conserved in a plasma (unlike the Boltzmann equation for neutral particles) because f_0 couples to the electric field through $\mathrm{d}f_0/\mathrm{d}t = -E\partial f_0/\partial v$. Evaluating the relative entropy for the Maxwell–Boltzmann distribution $f_0 = \pi^{-1/2}\mathrm{e}^{-v^2}$ in standard dimensionless variables gives

$$\begin{aligned}\mathcal{R}[\tilde{f}|f_0] &= \int_\Omega \mathrm{d}z \; \int_{-\infty}^{\infty} \mathrm{d}v \; \tilde{f}\log\tilde{f} - \tilde{f}\log f_0 - \tilde{f} + f_0 \\ &= \mathcal{H}[\tilde{f}] + \int_\Omega \mathrm{d}z \; \int_{-\infty}^{\infty} \mathrm{d}v \; \left(\frac{1}{2}\log\pi - 1\right)\tilde{f} + v^2\tilde{f} + f_0,\end{aligned} \tag{2.17}$$

so the free energy defined

$$\begin{aligned} W_{\text{exact}} &= \mathcal{R} + \int_\Omega \mathrm{d}z\ |E|^2 \\ &= \mathcal{H}[\tilde{f}] + \left(\frac{1}{2}\log\pi - 1\right) N + 2H + \int_\Omega \mathrm{d}z\ 1, \end{aligned} \tag{2.18}$$

is a conserved quantity. Approximating the relative entropy by its quadratic form (2.16) gives the quadratic expression

$$\begin{aligned} W &= W_f + W_E \\ W_f &= \int_\Omega \mathrm{d}z\ \int_{-\infty}^{\infty} \mathrm{d}v\ \frac{f^2}{2f_0} \\ W_E &= \int_\Omega \mathrm{d}z\ |E|^2, \end{aligned} \tag{2.19}$$

which may be expressed neatly in terms of the Fourier–Hermite expansion coefficients of f using Parseval's theorems (see section 3).

3. Fourier–Hermite spectral representation

We solve the Vlasov–Poisson system (2.5)–(2.7) using a Fourier–Hermite representation. In space we represent the distribution function with a Fourier series, properties of which are well known. In velocity space we expand the distribution function as the sum of Hermite functions. For this we introduce the Hermite polynomials H_m and re-normalized Hermite functions ϕ^m defined by

$$H_m(v) = (-1)^m \mathrm{e}^{v^2} \frac{\mathrm{d}^m}{\mathrm{d}v^m}\left(\mathrm{e}^{-v^2}\right), \qquad \phi^m(v) = \frac{H_m(v)}{\sqrt{2^m m!}}, \tag{3.1}$$

for $m = 0, 1, 2, \ldots$. The Hermite functions ϕ^m are orthonormal with respect to the Maxwellian weight $\mathrm{e}^{-v^2}/\sqrt{\pi}$, so that introducing the dual Hermite functions $\phi_m(v) = \mathrm{e}^{-v^2}\phi^m(v)/\sqrt{\pi}$ we have the bi-orthonormality condition

$$\int_{-\infty}^{\infty} \phi_n(v)\phi^m(v)\,\mathrm{d}v = \delta_{nm}, \quad \forall n \geqslant 0, m \geqslant 0. \tag{3.2}$$

Each ϕ_m satisfies the velocity space boundary condition $\phi_m(v) \to 0$ as $v \to \pm\infty$, and the set of dual Hermite functions is complete for functions that are analytic on a strip in the complex v plane and satisfy the decay condition $|f(v)| < c_1\mathrm{e}^{-c_2 v^2/2}$ for some constants $c_1 > 0$ and $c_2 > 1$ (Boyd 2001). The Hermite functions oscillate with characteristic wavelength $\pi(2/m)^{1/2}$ so that higher-order functions represent finer velocity space scales. Neighbouring modes are related by the recurrence relation

$$v\phi_m(v) = \sqrt{\frac{m+1}{2}}\phi_{m+1}(v) + \sqrt{\frac{m}{2}}\phi_{m-1}(v), \tag{3.3}$$

and velocity derivatives are related to a single neighbouring mode

$$\frac{\partial\phi_m}{\partial v} = -\sqrt{2(m+1)}\phi_{m+1}, \qquad \frac{\partial\phi^m}{\partial v} = \sqrt{2m}\phi^{m-1}. \tag{3.4}$$

We expand the distribution function in a series of dual Hermite functions and, to obtain a finite sum, truncate after the first N_m (slowest-oscillating) Hermite modes. This truncation is equivalent to a velocity space discretization on the roots of the Hermite

polynomial H_{N_m}. The spacing between these roots decreases like $1/\sqrt{N_m}$ as $N_m \to \infty$. However as the Vlasov–Poisson system is linear in velocity space, so there is no need to explicitly discretize in v.

3.1. *Discretized system*

We solve (2.5)–(2.7) using the Fourier–Hermite representation

$$f(z,v,t) = \sum_{m=0}^{N_m-1} \sum_{j=-N_\vartheta}^{N_\vartheta} a_{jm}(t) \mathrm{e}^{\mathrm{i}k_j z} \phi_m(v), \tag{3.5}$$

with inverse

$$a_{jm}(t) = \frac{1}{L} \int_{-\infty}^{\infty} \mathrm{d}v \int_0^L \mathrm{d}z \; f(z,v,t) \mathrm{e}^{-\mathrm{i}k_j z} \phi^m(v), \tag{3.6}$$

where $k_j = 2\pi j/L$. Thus the continuous function $f(z,v,t)$ is defined by a discrete, finite set of coefficients a_{jm}, which are implicitly a function of time. Putting (3.5) into the Vlasov–Poisson system (2.5)–(2.7) and applying the operator

$$\frac{1}{L} \int_{-\infty}^{\infty} \mathrm{d}v \int_0^L \mathrm{d}z \; \mathrm{e}^{-\mathrm{i}k_j z} \phi^m(v), \tag{3.7}$$

we derive the discrete system

$$\frac{\mathrm{d}a_{jm}}{\mathrm{d}t} + \mathrm{i}k_j \left(\sqrt{\frac{m+1}{2}} a_{j,m+1} + \sqrt{\frac{m}{2}} a_{j,m-1} \right) + \mathsf{N}_{jm} = -\sqrt{2} \hat{E}_j \delta_{m1}, \tag{3.8}$$

$$\hat{E}_j = -\mathrm{i}k_j \hat{\Phi}_j, \tag{3.9}$$

$$-k_j^2 \hat{\Phi}_j = a_{j0}, \tag{3.10}$$

where the nonlinear term N is the discrete Fourier convolution

$$\mathsf{N}_{jm} = \sqrt{2m} \sum_{j'=-N_\vartheta}^{N_\vartheta} \hat{E}_{j'} a_{j-j',m-1}, \tag{3.11}$$

and $\hat{E}$ and $\hat{\Phi}$ are the Fourier coefficients of E and Φ. The system (3.8)–(3.10) is an infinite moment hierarchy in Hermite space, where mode coupling results from particle streaming and velocity derivatives via the relations (3.3) and (3.4), and from the nonlinear term through the electric field. Because $\partial f_0/\partial v$ can be expressed in a Hermite series, the right-hand side of (3.8) is a finite number of source terms appearing at fixed Hermite modes m, and the system is closed but for the term a_{j,N_m+1} which appears in the particle streaming in the highest moment equation. The system (3.8)–(3.10) is also exactly the system obtained using a continuous Fourier–Hermite representation on an infinite spatial domain, but restricted to the discrete wavenumbers k_j and Hermite modes $m < N_m$.

Calculating the nonlinear term (3.11) directly for each grid point requires $O(N_m N_k^2)$ operations, but this is reduced to $O(N_m N_k \log N_k)$ operations if it is calculated pseudo-spectrally, *i.e.* via a grid in z-space using discrete Fourier transforms. For this we require a discrete version of (3.5) and (3.6). Specifically (3.5) must hold at every grid point $z_l = lL/N_k$,

$$f(z_l,v) = \sum_{m=0}^{N_m-1} \sum_{j=-N_\vartheta}^{N_\vartheta} a_{jm} \mathrm{e}^{\mathrm{i}k_j z_l} \phi_m(v), \tag{3.12}$$

and we must replace the inverse z-integral (3.6) with a finite sum of Fourier modes. The choice of uniform spatial grid $z_l = lL/N_k$ is motivated by the resolution of the identity for Fourier modes

$$\delta_{jj'} = \frac{1}{N_k} \sum_{l=0}^{N_k-1} \mathrm{e}^{2\pi \mathrm{i}(j-j')l/N_k} = \frac{1}{N_k} \sum_{l=0}^{N_k-1} \mathrm{e}^{\mathrm{i}(k_j - k'_j)lL/N_k}, \tag{3.13}$$

so that multiplying (3.12) by $\mathrm{e}^{-\mathrm{i}k_{j'}z_l}$ and summing over l we obtain

$$a_{jm} = \frac{1}{N_k} \sum_{l=0}^{N_k-1} \int_{-\infty}^{\infty} \mathrm{d}v \; f(z_l, v) \mathrm{e}^{-\mathrm{i}k_j z_l} \phi^m(v), \tag{3.14}$$

with the nonlinear term calculated as

$$\mathsf{N}_{jm} = -\mathrm{i}\sqrt{2m} \; \mathsf{F}_{jl} \left\{ \mathsf{F}^{-1}_{ln} \left(k_n \hat{\Phi}_n \right) \mathsf{F}^{-1}_{ln'} \left(a_{n',m-1} \right) \right\}, \tag{3.15}$$

where F is the discrete Fourier transform operator

$$\mathsf{F}_{jl} = \frac{1}{N_k} \sum_{l=0}^{N_k-1} \mathrm{e}^{-\mathrm{i}k_j z_l}, \qquad \mathsf{F}^{-1}_{ln} = \sum_{n=0}^{N_k-1} \mathrm{e}^{\mathrm{i}k_n z_l}. \tag{3.16}$$

3.1.1. *Discrete free energy equations*

We now obtain evolution equations for the quadratic free energies W_E, W_f (2.19). These have neat expressions in terms of the Fourier–Hermite coefficients obtained by inserting the spectral representation (3.5) into (2.19),

$$\begin{aligned} W_f &= \int_\Omega \mathrm{d}z \int_{-\infty}^{\infty} \mathrm{d}v \; \frac{f^2}{2f_0} = \frac{1}{2} \sum_{j=-N_\vartheta}^{N_\vartheta} \sum_{m=0}^{N_m} |a_{jm}|^2, \\ W_E &= \int_\Omega \mathrm{d}z \; |E|^2 = \sum_{j=-N_\vartheta}^{N_\vartheta} |\hat{E}_j|^2. \end{aligned} \tag{3.17}$$

Evolution equations for these are obtained by manipulating the moment equations (3.8)–(3.10). Multiplying the $m = 0$ moment equation by a^*_{j0}/k_j^2, using (3.9) and (3.10) to insert the electric field, adding the result to its complex conjugate and summing over j we obtain

$$\frac{\mathrm{d}W_E}{\mathrm{d}t} + \mathcal{F} = 0, \tag{3.18}$$

where

$$\mathcal{F} = \sqrt{2} \; \mathrm{Re} \left(\sum_{j=-N_\vartheta}^{N_\vartheta} \frac{\mathrm{i}a^*_{j0}a_{j1}}{k_j} \right), \tag{3.19}$$

is a flux between the first two Hermite moments. Similarly, multiplying (3.8) by a^*_{jm}, adding the result to its complex conjugate, and summing over all m and j, we obtain

$$\frac{\mathrm{d}W_f}{\mathrm{d}t} - \mathcal{F} + \mathcal{T} = \mathcal{C}, \tag{3.20}$$

where

$$\mathcal{T} = \mathrm{Re}\left(\sum_{j=-N_\vartheta}^{N_\vartheta}\sum_{m=0}^{N_m} a_{jm}^* \mathsf{N}_{jm}\right), \tag{3.21}$$

$$\mathcal{C} = \mathrm{Re}\left(\sum_{j=-N_\vartheta}^{N_\vartheta}\sum_{m=0}^{N_m} a_{jm}^* C_{jm}\right), \tag{3.22}$$

are the nonlinear term viewed as a free energy source and the collisional sink of free energy.

Combining (3.18) and (3.20) we have the global budget equation

$$\frac{\mathrm{d}}{\mathrm{d}t}\left(W_f + W_E\right) + \mathcal{T} = \mathcal{C} \tag{3.23}$$

In the linear case without collisions ($\mathcal{T} = \mathcal{C} = 0$), this expresses the exact discrete conservation of the truncated free energy $W = W_f + W_E$. Nonlinearly, $\mathcal{T}$ accounts for the terms omitted in the linearization of free energy W_{exact} (2.18).

Finally, equation (3.18) shows that W_E only changes through the flux term $\mathcal{F}$. We show later (section 4.2.2) that this term represents net the flux of free energy through Hermite space. Therefore the electric field only decays or grows as the result of net forwards or backwards Hermite flux respectively.

3.2. *Algorithm description*

We now discuss details of the algorithm to solve (3.8)–(3.10). These equations may be combined and written schematically as

$$\frac{\mathrm{d}\mathsf{a}}{\mathrm{d}t} = \mathcal{A}\left[\mathsf{a}\right], \tag{3.24}$$

where a denotes the coefficients a_{jm}. The algorithm has two main steps: forming the right-hand side $\mathcal{A}$, and numerically integrating $\mathcal{A}$ in time to find the coefficients a. Time integration is performed by third-order Adams–Bashforth as discussed in section 3.2.1. To form $\mathcal{A}$, we must determine the electric field, calculate the nonlinear term, and properly treat the fine scales that appear in space and velocity space due to the nonlinear term and particle streaming respectively. These are discussed in sections 3.2.2–3.2.4. We consider the parallelization and communication patterns in the code in section 3.2.5.

As noted in section 2, the Vlasov–Poisson system is very similar to the long-wavelength limit of gyrokinetics. Therefore we solve using SpectroGK, a full 5D gyrokinetics code which also features a mode for solving in the (1+1)D long wavelength limit. To solve the Vlasov–Poisson system rather than gyrokinetics, we make two modifications to SpectroGK which are described in section 3.2.5 along with details of the parallelization scheme. These changes do not affect the key algorithms or structure of the code and so the test problems in section 4 act to validate SpectroGK.

3.2.1. *Time integration*

The solution of (3.24) is approximated using the explicit third-order Adams–Bashforth scheme,

$$\mathsf{a}^{i+1} = \mathsf{a}^i + \Delta t\left(\frac{23}{12}\mathcal{A}\left[\mathsf{a}^i\right] - \frac{4}{3}\mathcal{A}\left[\mathsf{a}^{i-1}\right] + \frac{5}{12}\mathcal{A}\left[\mathsf{a}^{i-2}\right]\right), \tag{3.25}$$

where a^i denotes the coefficients a_{jm} at the ith time level, and Δt is the timestep. SpectroGK also implements a variable time-spacing version of this formula to allow changing the timestep during execution.

The advantages of third-order Adams–Bashforth are given in Durran (1991, 1999). It is stable and accurate for non-dissipative wave phenomena, with fourth-order errors in amplitude and wave speed. It is also appropriate for problems like ours where the calculation of $\mathcal{A}$ dominates the computation work. Durran (1991) defines the "efficiency factor" of an integration scheme, the maximum stable timestep in an oscillatory test problem divided by the number of evaluations of $\mathcal{A}$ per timestep. By this measure Adams–Bashforth is the most efficient third-order scheme, as while it has a smaller stable timestep than other schemes such as Runge–Kutta, it only requires one $\mathcal{A}$ evaluation per timestep.

The main disadvantage of third-order Adams–Bashforth is that two previous timestep operators must be stored. This is potentially a problem as the operators are each the same size as the total problem size; however this is not limiting in the (1+1)D Vlasov–Poisson system.

One must also ensure that the scheme is third order accurate: as (3.25) uses three past values at each timestep, we must amend the scheme for the first and second timesteps where fewer past values are available. For these two timesteps we use explicit Euler and second-order Adams–Bashforth timestep respectively. In principle, the use of explicit Euler makes the global time integration error second order (the local truncation error is first order, but as explicit Euler is only used once, the error does not accumulate over $\sim 1/\Delta t$ timesteps). In practice however, the error in explicit Euler time integration is insignificant relative to other errors.

3.2.2. *Field solve*

The electric field for use in $\mathcal{A}$ is readily obtained from (3.9) and (3.10): if $k_j = 0$ then $E_j = 0$, otherwise $E_j = \mathrm{i}a_{j0}/k_j$. The truncated Hermite expansion is equivalent to a discretization in v-space on a grid the roots of H_{N_m}, and so a_{j0} is equal to the zeroth moment of the distribution function obtained via $(2N_m - 1)$th order Gauss–Hermite quadrature. However unlike v-space discretizations which require a sum over all grid points, the evaluation of the field in Hermite space requires only the coefficient a_{j0}. This has communication benefits discussed in section 3.2.5.

3.2.3. *Nonlinear term*

We calculate the nonlinear term (3.15) using the product of discrete Fourier transforms. As derived in section 3.1, the discrete wavenumbers and z-grid are

$$k_j = 2\pi j/L, \qquad z_l = lL/N_k. \tag{3.26}$$

We use the FFTW library (Frigo & Johnson 2005), which implements unnormalized discrete Fourier transforms, *i.e.* (3.16) but without the factor $1/N_k$ in the first transform. Note that with the normalization in (3.16) the forward transform of $\mathrm{e}^{\mathrm{i}k_j z_l}$ has magnitude one.

With this pseudospectral approach, the problem of Fourier aliasing occurs. The product of inverse transforms in (3.15) is a sum over Fourier modes $\mathrm{e}^{\mathrm{i}(k_n + k_{n'})z_l}$. When $k_n + k_{n'} > k_{N_\vartheta}$ the largest wavenumber in the simulation, its contribution to the nonlinear term should be neglected. However as the discrete Fourier transform is periodic, this mode contributes to the Fourier transform at the wavenumber $k_n + k_{n'} - k_{N_\vartheta}$. This spurious appearance of high wavenumber contributions in the low wavenumbers is called aliasing. Dealiasing is often performed by the two-thirds rule, a Fourier filter where the Fourier coefficients for the highest third of wavenumbers are set to zero before the nonlinearity

is calculated. For quadratic nonlinearities such as the Fourier convolution (3.11), this removes all spurious modes as all modes with $|k_n + k_{n'}| > k_{N_\vartheta}$ remap onto wavenumbers that are neglected from the simulation (Orszag 1971; Boyd 2001).

The two-thirds rule works well, but costs one-third of the resolution. In addition, the sharp transition from unmodified coefficients to zeroed coefficients acts like a reflecting boundary condition in wavenumber space. This causes error in the highest resolved wavenumbers unless the Fourier coefficients are negligible at the point the filter is imposed. To ensure this is the case we multiply the distribution by the Hou–Li filter (Hou & Li 2007)

$$\exp\left(-36(|k|/\max(k))^{36}\right), \tag{3.27}$$

before the calculation of the nonlinear term. In fact, this damps the highest modes so strongly that both smoothing and dealiasing is effected. Indeed using the Hou–Li filter instead of two-thirds filtering allows one to keep 12–15% more Fourier modes (Hou & Li 2007).

3.2.4. *Recurrence*

The particle streaming term $v\partial f/\partial z$ is a phase space shear that causes infinitesimally small scale structure to form in velocity space. For any discretization, these structures become finer than grid-scale after some finite, resolution-dependent time. The discretization fails to capture this structure and is invalid after this time.

In Hermite space, particle streaming corresponds to nearest-neighbour mode coupling due to the recurrence relation (3.3), where each mode represents the velocity space scale $\sim \pi(2/m)^{1/2}$. The moment hierarchy is not closed as the mth equation depends on the $(m+1)$th Hermite mode. To truncate the hierarchy we set $a_{jm} = 0$ for all $m \geqslant N_m$, which determines the finest resolved velocity scale, $\sim \pi(2/N_m)^{1/2}$. In the highest moment equation, truncation forces $a_{jN_m} = 0$, *i.e.* forces streaming to finer scales to vanish. Thus $a_{N_m} = 0$ is like a hard-wall boundary condition for quantities like $|a_{jm}|^2$, the contribution of Fourier–Hermite mode (j, m) to the free energy (2.19). In the linear system one may observe an initial forward flux of free energy in Hermite space from large to small scales, a reflection at the point $m = N_m$, and a subsequence backwards flow of free energy. Recurrence occurs when this spuriously reflected free energy reappears in the low moments that represent the physical quantities. Recurrence is so called because this returning free energy causes a sudden increase in the magnitude of a previously decaying quantity, such as the Landau-damped electrostatic potential.

Schekochihin *et al.* (2014) showed that the Hermite coefficients decompose as the sum of forward and backward propagating modes. Linearly these modes decouple apart from at the boundary $m = N_m$, where incoming forward modes excite the backwards propagating modes which cause recurrence. Recurrence is therefore prevented by damping the distribution function with a filter or collision operator so that $a_{jN_m} = 0$. For low resolution ($N_m \sim 10$), the damping must be smooth across Hermite space (*i.e.* algebraic in m), and hypercollisional operators such as the iterated Lénard–Bernstein operator (Lénard & Bernstein 1958)

$$-\nu(m/N_m)^\alpha a_{jm}, \tag{3.28}$$

are effective. In linear simulations, the critical collision frequency ν^* decreases with resolution as $\nu^* \sim 1/N_m^\alpha$. Thus the factor $1/N_m^\alpha$ allows a constant ν to be used for different resolutions. We have also used this operator for higher resolution and nonlinear simulations of the Vlasov–Poisson system; however the collision frequency ν must be tuned with resolution making convergence studies awkward. Instead we smooth velocity space

with the Hou–Li-type filter

$$\exp\left(-36(m/(N_m-1))^{36}\right). \tag{3.29}$$

While this is too sharp for low resolutions (small N_m), it is sufficiently smooth for high resolutions, and yields exponential convergence as demonstrated in section 4.2.1.

3.2.5. SpectroGK

The system (3.8)–(3.10) is implemented using a reduced-dimension version of the gyrokinetics code SpectroGK. For SpectroGK to solve the Vlasov–Poisson system, we make two modifications. Firstly we replace the gyrokinetic quasineutrality condition (1.2c) with Gauss' law (2.7). As the code is spectral in Fourier space, this change is trivial. Secondly we insert the nonlinear term (3.15) which is absent in gyrokinetics (at the order solved by SpectroGK).

The SpectroGK parallelization scheme is described in detail in Parker *et al.* (2014). The basic idea is to divide the five-dimensional distribution function evenly among processors, while forcing all the parallel wavenumbers for a given phase space point to be local to a processor. Each processor also has a copy of the smaller, three-dimensional electromagnetic field. For the (1+1)D Vlasov–Poisson system we therefore parallelize over m while keeping k local. This is optimal. The main potential source of communication is in the nonlinear term (3.15) where the Fourier transforms are sums over all k at a fixed m. By keeping all k on processor, communication is entirely eliminated from this term.

Besides the nonlinear term, the equations are largely local in phase space, and only two parts require communication. Firstly the mode coupling and nonlinear term in (3.8) require communication of neighbouring Hermite modes when these fall on different processors. This is small point-to-point communication and is entirely vectorized in k. Secondly, in the discrete Poisson equation (3.10) the electric field is calculated on the processor which holds a_{j0} and is then sent to all other processors. Here the Hermite spectral method is preferable to velocity grid discretizations, where contributions to a sum approximating the integral in (2.7) must be sent and received by each processor before the broadcast of the electric field.

4. Numerical results

We present the solution of the linearized and nonlinear Vlasov–Poisson system with SpectroGK. In the absence of exact nonlinear solutions, we benchmark SpectroGK against other codes under grid refinement, for two standard nonlinear test problems, nonlinear Landau damping and the two stream instability.

Following convention, the initial conditions unless otherwise stated are

$$\tilde{f}(v) = f_0(v) + A\cos(kz)f_0(v), \tag{4.1}$$

where $A = 0.5$, $k = 0.5$, and we use a box length $L = 4\pi$ so that wavenumbers are half-integers.

4.1. *Linear Landau damping*

The linearized system obtained by neglecting the term $-E\partial f/\partial v$ in (2.5) exhibits Landau damping, according to the dispersion relation

$$D(\omega) = ik^3 + 2ik + 2i\omega Z(\omega/k) = 0, \tag{4.2}$$

where $Z(\zeta) = \pi^{-1/2}\int e^{-v^2}/(v-\zeta)\,\mathrm{d}v$ is the plasma dispersion function (Fried & Conte 1961). This has the property that roots ω appear in frequency pairs $\pm\omega_R + i\gamma$ corre-

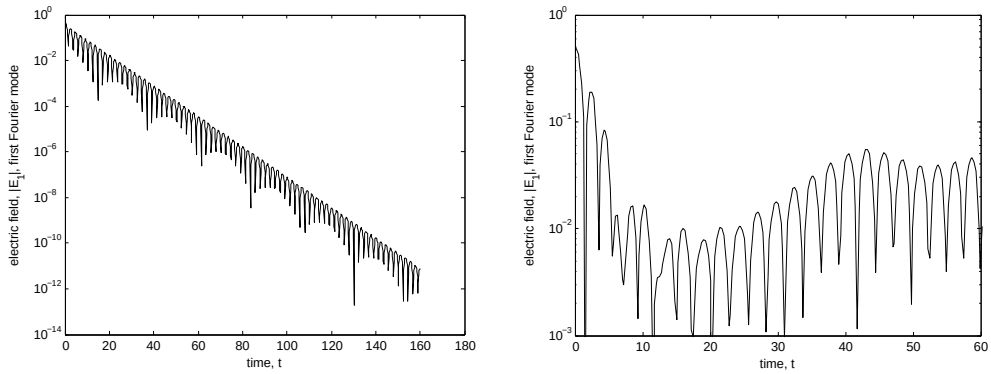

(a) Linear (b) Nonlinear

FIGURE 1. The first electric field Fourier mode versus time.

sponding to left and right travelling waves. Thus there are two dominant modes with equal growth rate and opposite frequency.

The discretized system is equivalent to the matrix initial value problem

$$\frac{\partial f}{\partial t} = Mf, \tag{4.3}$$

with timestep operator M. The exact solution is obtained in terms of eigenvalues $i\omega$ and eigenvectors x of M,

$$f(z, v, t) = \sum_{l=1}^{N_m} \alpha_l x_l e^{i(k_j z - \omega_l t)}. \tag{4.4}$$

The coefficients $\alpha_l = y_l^* \beta / (y_l^* x_l)$ where y_l is the lth eigenvector of the adjoint matrix M^*, and β is the initial value of the distribution function in velocity space. The dominant eigenvalues of M also occur in the frequency pair $\pm\omega_R + i\gamma$. Generic initial conditions excite both dominant eigenmodes and after sufficient long time leads to an oscillation with frequency $2\omega_R$ via the interference pattern of the two modes

$$|\varphi|^2 \sim |\varphi_1 e^{-i\omega_R t + \gamma t} + \varphi_2 e^{i\omega_R t + \gamma t}|^2 = \left(|\varphi_1|^2 + |\varphi_2|^2 + 2\mathrm{Re}(\varphi_1^* \varphi_2 e^{2i\omega_R t})\right) e^{2\gamma t}. \tag{4.5}$$

Thus we may also determine the frequency of the dominant mode from the initial value problem.

In Figure 1(a) we plot the $k = 0.5$ mode for a linear simulation with the Hou–Li filter (3.29) applied in Hermite space. The frequency $\omega_R = 1.415$ and damping rate $\gamma = -0.153$ are in agreement with Cheng & Knorr (1976). In Figure 2(a) we plot the corresponding free energy time trace: the free energies of the electric field W_E and distribution function W_f, and the time-integrated collisional sink $\mathcal{S}$. After an initial transient, by $t = 20$ the system enters the collisionless regime in which W_E decays at the Landau rate with a superimposed oscillation due to two mode interference, while W_f oscillates in antiphase to W_E without decaying. This is reminiscent of Landau's Laplace transform solution (Landau 1946), and in contrast to the regime one might expect where W_E would not decay linearly until W_f was also linearly decaying.

The collisionless regime lasts until the free energy in the distribution function reaches collisional scales and is damped. The system enters the asymptotic regime where both W_E and W_f decay at the Landau rate. This behaviour is the same as that described by Ng

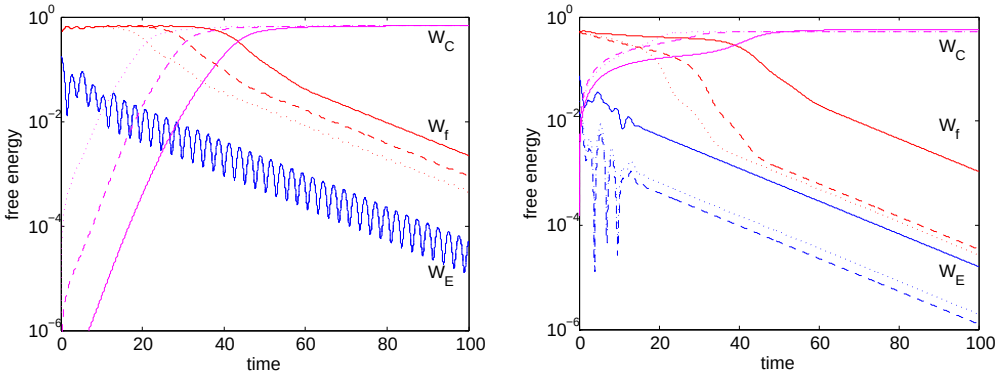

(a) All modes excited. (b) One dominant mode removed.

FIGURE 2. Free energy contributions in the linear case. Line style corresponds to resolution: $N_m = 128$ (dotted), $N_m = 256$ (dashed), $N = 512$ (unbroken).

et al. (1999) for systems with weak Fokker–Planck collisions. The time for free energy to reach collisional scales increases with resolution so that the onset of the eigenmode regime may be delayed by increasing the number of Hermite modes, as shown in Figure 2(a).

Both W_E and W_f oscillate as they decay due to two-mode interference as in (4.5). We obtain smooth decay by choosing initial conditions which do not project onto one of the dominant modes. Now the free energy traces are smooth (Figure 2(b)) with the dominant mode a single travelling wave.

4.2. *Nonlinear Landau damping*

We now present simulations of nonlinear Landau damping, which has been treated extensively in the literature (*e.g.* Grant & Feix 1967; Cheng & Knorr 1976; Zaki *et al.* 1988; Nakamura & Yabe 1999; Filbet *et al.* 2001; Zhou *et al.* 2001; Heath *et al.* 2012). We benchmark SPECTROGK by reproducing known results and demonstrating convergence, before giving a description of the system via its Hermite space behaviour.

The electric field for the dominant Fourier mode at early times is given in Figure 1(b), and longer time traces of the four lowest modes are plotted in Figure 3. These are in agreement with previous simulations (*e.g.* Heath *et al.* 2012).

We also plot time slices of the perturbed distribution f in (z, v)-space in Figure 4. These show phase space shearing at early-times leading to a striped, highly-oscillatory pattern in velocity space that is characteristic of phase mixing (and is indeed similar to the linear Landau damping case plotted in Heath *et al.* 2012, Figure 3). Here however nonlinear effects are visible as the stripes are not straight lines, but are wave-like with contours of the distribution function oscillating in z with wavenumber $k = 0.5$. The waves at larger velocities oscillate with larger amplitude in v. At about $t = 30$, the oscillations in the region $|v| \in (1, 2)$ roll up, forming vortex-like structures which propagate in the direction of the shearing (see Figure 4(e)). By $t = 60$ (Figure 4(f)), shearing has elongated these structures to be on the box scale, and they persist, flowing in the shearing direction in the region $|v| \in (1, 2)$. The region $v \in (-1, 1)$ retains the striped phase mixed pattern, but also has a clear oscillation with wavenumber $k = 0.5$.

In Figure 5(a) we plot the free energy contributions W_E, W_f, W_N and $\mathcal{S}$ and in Figure 5(b) plot their respective time derivatives $\dot{W}_E$, $\dot{W}_f$, $\mathcal{T}$ and $\mathcal{C}$. At long times, the free energies reach a steady state. In particular the collisional sink $\mathcal{C}$ tends to zero so that no free energy is removed from the system. Thus at long times free energy is

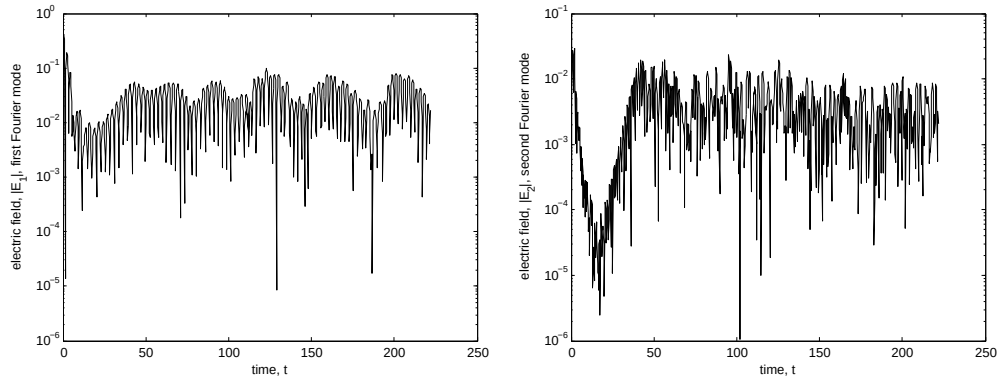

(a) $k = 0.5$ (b) $k = 1.0$

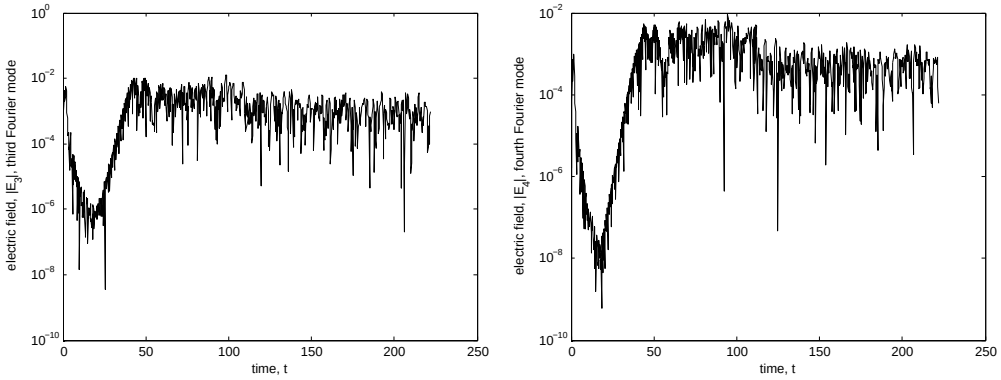

(c) $k = 1.5$ (d) $k = 2.0$

FIGURE 3. Electric field versus time for the first four Fourier modes.

exchanged between W_f, W_N and W_E. Moreover we see from Figure 5(b) that $\dot{W}_f$ and $\mathcal{T}$ are approximately equal, and thus there are only small changes in the electric field free energy as $\dot{W}_E \approx \dot{W}_f - \mathcal{T}$.

4.2.1. *Convergence*

We show convergence behaviour by making a series of runs, repeatedly doubling resolution: N_m from 32 to 4096, and $(N_k - 1)$ from 16 to 256. At a fixed time, we compare the Fourier–Hermite coefficients of a run to those of the best resolved run $(N_k, N_m) = (257, 4096)$. That is if a_{jm} and $\bar{a}_{jm}$ are the Fourier–Hermite modes of the two runs, we define the error

$$\sum_{j=-N_\vartheta^*}^{N_\vartheta^*} \sum_{m=0}^{N_m^*} |a_{jm} - \bar{a}_{jm}|^2, \tag{4.6}$$

where N_ϑ^*, N_m^* define which modes are included in the comparison. Since both sets of coefficients are subject to resolution-dependent Fourier filtering, we consider only the modes which are unaffected by filtering in both runs. We therefore take $N_\vartheta^* = \lfloor 2N_\vartheta/3 \rfloor$ and $N_m^* = \lfloor 2N_m/3 \rfloor$, for (N_ϑ, N_m) of the lesser resolved run. In Figure 6 we plot Hermite spectra for different resolutions to illustrate which modes achieve convergence.

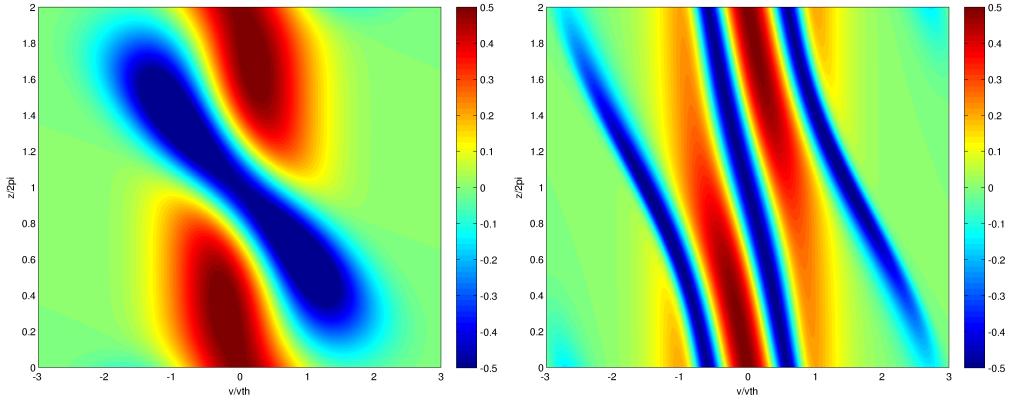

(a) $t = 1$ (b) $t = 5$

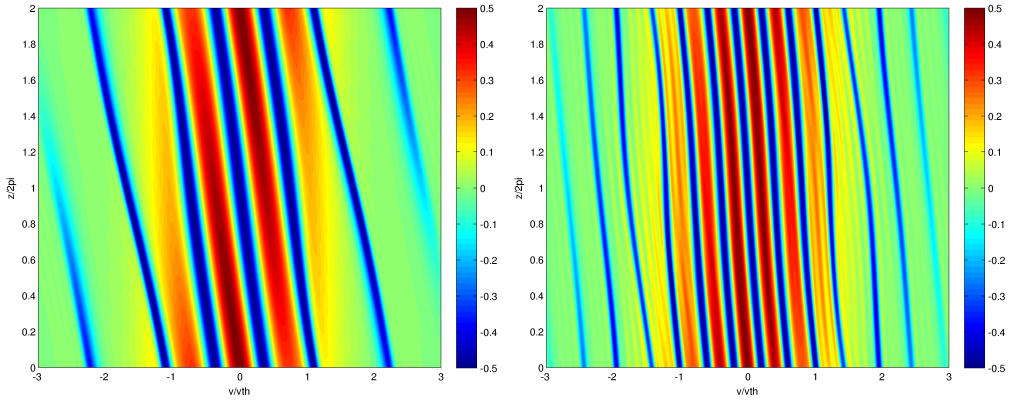

(c) $t = 10$ (d) $t = 20$

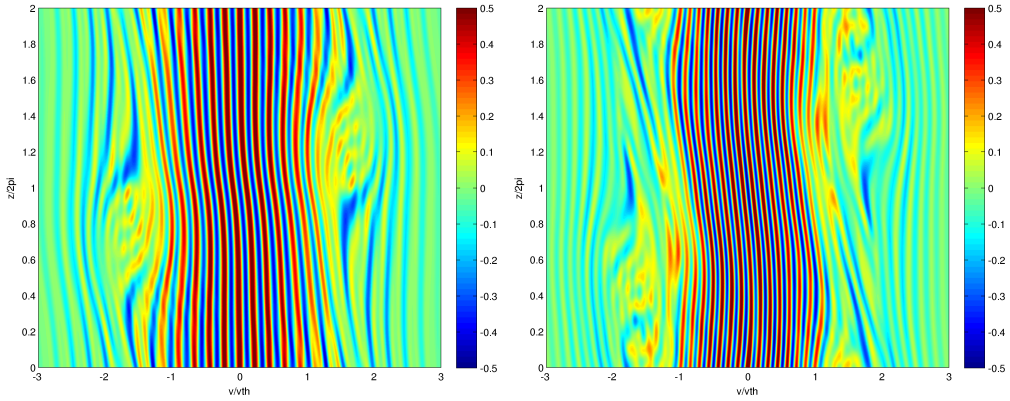

(e) $t = 40$ (f) $t = 60$

FIGURE 4. Time slices of the perturbed distribution function (3.12) in (z, v) space with resolution $(N_k, N_m) = (257, 2048)$. The distribution is plotted on z-collocation points using the discrete Fourier transform of the Fourier–Hermite coefficients. As the Hermite transform is spectral, any velocity grid is permitted, and we plot on a grid of 2048 points with $v \in [-3, 3]$.

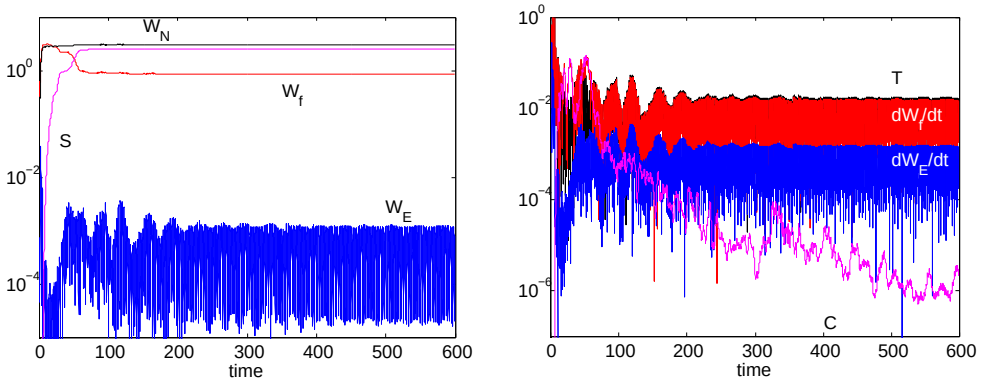

FIGURE 5. Free energy time traces for the nonlinear system.

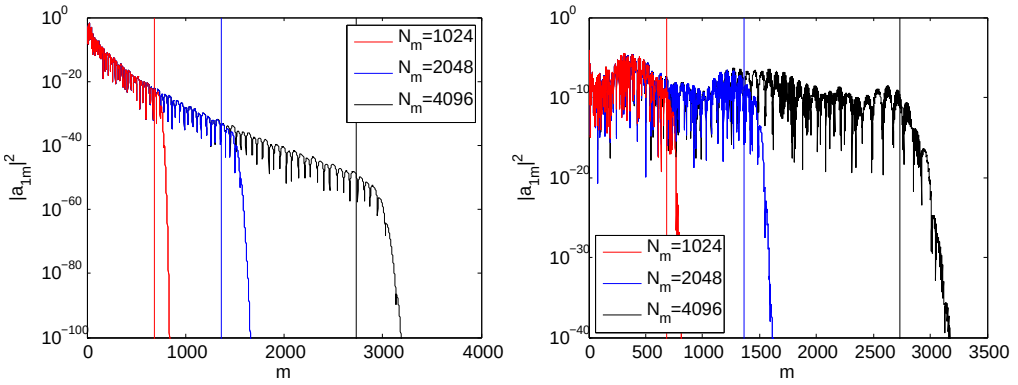

(a) (b)

FIGURE 6. Hermite spectra with Hou–Li filtering at $t = 10$ (left) and $t = 40$ (right). The vertical lines are at $m = 2N_m/3$ for each resolution. All spectra are for wavenumber k_1 and have $N_k = 257$.

The difference in spectral coefficients (without mode selection) is related to the squared difference of the distribution functions via Parseval's theorem

$$\sum_{j=-N_\vartheta}^{N_\vartheta} \sum_{m=0}^{N_m} |a_{jm} - \bar{a}_{jm}|^2 = \frac{1}{N_k} \sum_{l=0}^{N_k-1} \int \mathrm{d}v \, \frac{|f(z_l, v) - \bar{f}(z_l, v)|^2}{f_0}, \tag{4.7}$$

where f and $\bar{f}$ are the distribution functions corresponding to a_{jm}, $\bar{a}_{jm}$. Thus the error (4.6) is similar to the error in the distribution function on collocation points in (z, v)-space, but with an extra factor of $1/f_0$ which exaggerates errors in the velocity tail of the distribution.

In Figure 7 we plot the error for two times, $t = 10$ and $t = 40$, which correspond to phase space diagrams Figures 4(c) and 4(e). At the earlier time $t = 10$, the behaviour is similar to the linear case. There is little structure in z and once we have enough Fourier modes to capture this ($N_k = 33$), the error does not decrease with N_k. While there is finer structure in v, this is captured by 256 Hermite modes, and as with N_k, increasing N_m beyond this point does not reduce the error.

The later time $t = 40$ corresponds to the top of the roll-over in the electric field (see

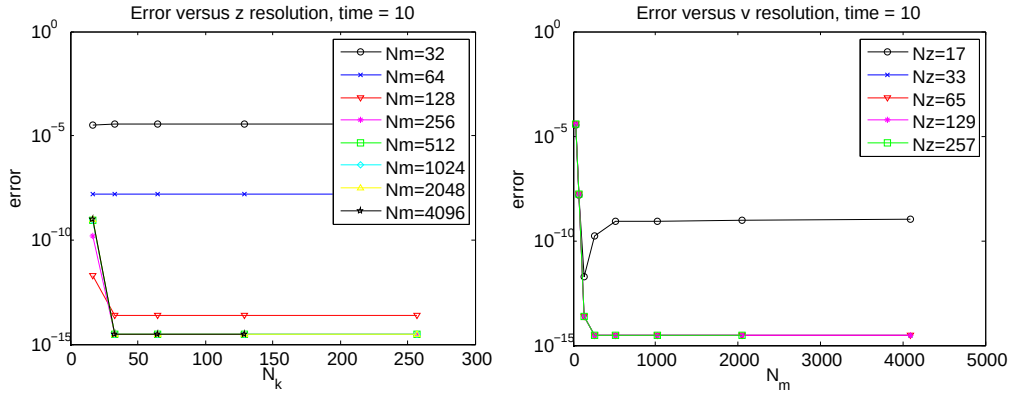

(a) Convergence with N_k, $t = 10$

(b) Convergence with N_m, $t = 10$

(c) Convergence with N_k, $t = 40$

(d) Convergence with N_m, $t = 40$

FIGURE 7. Convergence.

Figure 1(b)). The physical space structure is still captured by a small number of Fourier modes after which there is no improvement in convergence. In Hermite space, the scheme converges exponentially in N_m once at least 33 Fourier modes are used.

4.2.2. *Hermite flux*

We now describe the behaviour of the system in Fourier–Hermite phase space with a view to explaining two nonlinear effects: firstly that after its initial decay, the electric field grows in the absence of linear instability; and secondly that the electric field does not decay at long times.

The magnitude of the coefficients $|a_{jm}|^2$ are contributions to the leading order relative entropy (2.16) from each Fourier–Hermite mode

$$\mathcal{R}[\tilde{f}|f_0] = \int_{-\infty}^{\infty} \mathrm{d}z \int_{-\infty}^{\infty} \mathrm{d}v \, \frac{f^2}{2f_0} = \sum_{m=0}^{N_m-1} \sum_{j=-N_\vartheta}^{N_\vartheta} |a_{jm}|^2. \tag{4.8}$$

Moreover the coefficients may be used to describe the flow of relative entropy in Fourier–Hermite space. Zocco & Schekochihin (2011) studied the flow of free energy in a reduced gyrokinetic model, and showed that by introducing $\tilde{a}_{jm} = (\mathrm{i}\,\mathrm{sgn}\,k_j)^m a_{jm}$, particle streaming is a Hermite space flux. Applying this transform for $m > 1$ in the linearization

of (3.8) we obtain

$$\frac{1}{2}\frac{\partial \tilde{a}_{jm}^2}{\partial t} + \left(\Gamma_{j,m+1/2} - \Gamma_{j,m-1/2}\right) = 0, \tag{4.9}$$

where the Hermite flux is

$$\Gamma_{j,m-1/2} = |k_j|\sqrt{m/2}\ \tilde{a}_{jm}\tilde{a}_{j,m-1} = k_j\sqrt{m/2}\ \mathrm{Im}\left(a_{jm}^* a_{j,m-1}\right), \tag{4.10}$$

and the coefficients $\tilde{a}_{jm}$ are real. The flux equation (4.9) may be approximated by

$$\frac{1}{2}\frac{\partial \tilde{a}_{jm}^2}{\partial t} + \frac{\partial \Gamma_{jm}^{SV}}{\partial m} = 0, \tag{4.11}$$

with the flux defined as

$$\Gamma_{jm}^{SV} = |k_j|\sqrt{m/2}\ \tilde{a}_{jm}^2 = |k_j|\sqrt{m/2}\ |a_{jm}|^2. \tag{4.12}$$

Equation (4.11) may be written

$$\left(\frac{1}{2}\frac{\partial}{\partial t} + |k_j|\frac{\partial}{\partial\sqrt{2m}}\right)\left(\sqrt{2m}\tilde{a}_{jm}^2\right) = 0, \tag{4.13}$$

so that free energy propagates along characteristics $m = 2|k_j^2|(t-t_0)^2$. For eigenfunctions in time $\mathrm{d}|a_{jm}|^2/\mathrm{d}t = 2\gamma_j|a_{jm}|^2$, (4.11) gives the spectrum

$$|a_{jm}|^2 = \frac{C_j}{\sqrt{2m}}\exp\left(-\frac{2\sqrt{2}\gamma_j m^{1/2}}{|k|}\right), \tag{4.14}$$

for constants C_j, which is in excellent agreement with numerically-calculated linear spectra (Parker & Dellar 2014).

The approximation $\Gamma = \Gamma^{SV}$ holds provided that $\tilde{a}_{jm}$ is slowly varying in m in the sense that $\tilde{a}_{jm} \approx \tilde{a}_{j,m+1}$; equation (4.9) also supports alternating solutions with $\tilde{a}_{jm} \approx -\tilde{a}_{j,m+1}$. Therefore Schekochihin *et al.* (2014, see also Kanekar *et al.* (2014)) introduced the decomposition $\tilde{a}_{jm} = \tilde{a}_{jm}^+ + (-1)^m\tilde{a}_{jm}^-$, where

$$\tilde{a}_{jm}^+ = \frac{\tilde{a}_{jm} + \tilde{a}_{j,m+1}}{2}, \qquad \tilde{a}_{jm}^- = (-1)^m\frac{\tilde{a}_{jm} - \tilde{a}_{j,m+1}}{2}, \tag{4.15}$$

are both continuous in m. Substituting these into (4.9) we obtain

$$\begin{aligned}\frac{1}{2}\frac{\partial\left(\tilde{a}_{jm}^{\pm}\right)^2}{\partial t} &\pm \frac{|k_j|}{2}\left((s_{m+2}+s_{m+1})\tilde{a}_{j,m+1}^{\pm}\tilde{a}_{jm}^{\pm} - (s_{m+1}+s_m)\tilde{a}_{j,m-1}^{\pm}\tilde{a}_{jm}^{\pm}\right)\\ &\pm \frac{|k_j|(-1)^m}{2}\left((s_{m+2}-s_{m+1})\tilde{a}_{j,m+1}^{\mp}\tilde{a}_{jm}^{\pm} - (s_{m+1}-s_m)\tilde{a}_{jm}^{\pm}\tilde{a}_{j,m-1}^{\mp}\right) = 0,\end{aligned} \tag{4.16}$$

where $s_m = \sqrt{m/2}$ and the differences $s_{m+2} - s_{m+1}$ and $s_m - s_{m-1}$ are both $O(1/\sqrt{m})$. Thus for large m, the particle streaming is always a flux, but in a different direction for $\tilde{a}^+$ and $\tilde{a}^-$. The "phase-mixing" mode $\tilde{a}^+$ propagates from low to high m, while the "un-phase-mixing" mode $\tilde{a}^-$ propagates from high to low m.

Comparing the true Hermite flux Γ to the approximation Γ^{SV}, by defining the normalized flux

$$\hat{\Gamma}_{jm} = \frac{\Gamma_{jm}}{\Gamma_{jm}^{SV}} = \frac{\mathrm{sgn}\ k_j\ \mathrm{Im}\left(a_{j,m+1}^* a_{jm}\right)}{|a_{jm}|^2} = \frac{\tilde{a}_{j,m+1}\tilde{a}_{jm}}{\tilde{a}_{jm}^2} = \frac{(\tilde{a}_{jm}^+)^2 - (\tilde{a}_{jm}^-)^2}{(\tilde{a}_{jm}^+ + (-1)^m\tilde{a}_{jm}^-)^2}, \tag{4.17}$$

we see that the approximation $\Gamma \approx \Gamma^{SV}$ is valid when the $\tilde{a}^+$ mode is dominant; otherwise significant amounts of $\tilde{a}^-$ modifies the streaming. We therefore use the normalized Hermite flux to describe the transfer of free energy in phase space. This quantity is of particular interest in determining the behaviour of the electric field, as we recall from section 3.1.1 that the electric field only grows or decays as the result of net Hermite flux.

The nonlinear Vlasov–Poisson system (3.8)–(3.10) is written in terms of $\tilde{a}^\pm$ as

$$\frac{\partial \tilde{a}^\pm_{jm}}{\partial t} + S^\pm_{jm} + B^\pm_{jm} + N^\pm_{jm} = 0, \tag{4.18}$$

where the streaming term is

$$\begin{aligned} S^\pm_{jm} = &\pm \frac{|k_j|}{2}\left((s_{m+2}+s_{m+1})\tilde{a}^\pm_{j,m+1} - (s_{m+1}+s_m)\tilde{a}^\pm_{j,m-1}\right) \\ &\pm \frac{|k_j|(-1)^m}{2}\left((s_{m+2}-s_{m+1})\tilde{a}^\mp_{j,m+1} - (s_{m+1}-s_m)\tilde{a}^\mp_{j,m-1}\right) = 0, \end{aligned} \tag{4.19}$$

the Boltzmann response is

$$B^\pm_{jm} = \mp \frac{\delta_{m0}+\delta_{m1}}{|k_j|\sqrt{2}}\left(\tilde{a}^+_{j0} + \tilde{a}^-_{j0}\right), \tag{4.20}$$

and the nonlinear term is

$$N^\pm_{jm} = \pm \sum_{j'=-N_\vartheta}^{N_\vartheta} i\hat{E}_{j-j'}\left[(D^{m+1}_{jj'} + D^m_{jj'})\tilde{a}^\pm_{j',m-1} + (-1)^m(D^{m+1}_{jj'} - D^m_{jj'})\tilde{a}^\mp_{j',m-1}\right], \tag{4.21}$$

where the electric field may be written in terms of $\tilde{a}^\pm$ as

$$i\hat{E}_j = \begin{cases} -\frac{\tilde{a}^+_{j0}+\tilde{a}^-_{j0}}{k_j}, & j \neq 0, \\ 0, & j = 0, \end{cases} \tag{4.22}$$

and where $D^m_{jj'} = \sqrt{m/2}(\text{sgn } k_j)^m(\text{sgn } k_{j'})^{m-1}$. Again the difference $D^{m+1}_{jj'} - D^m_{jj'}$ is $O(1/\sqrt{m})$.

In Figures 8 and 9 we plot the Hermite spectra $(\tilde{a}^\pm)^2$ against Hermite index and time for the first wavenumber $k = 0.5$ in the linear and nonlinear systems. In the linear system the equations for $\tilde{a}^\pm$ decouple, except for the Boltzmann response term at $m = 0$ and $m = 1$, and for the $O(1/\sqrt{m})$ cross-coupling term in the streaming. Moreover the modes $\tilde{a}^\pm$ propagate along characteristics $m = \pm 2k^2(t-t_0)^2$. We observe this behaviour in Figures 8. In the linear case with the Hou–Li filter (Figures 8a,b) the free energy fluxes forward along very clear characteristics $m = 2k^2(t-t_0)^2$ until reaching collisional scales where it is damped. The decoupling is not perfect as there is some forward propagation observed in the $\tilde{a}^-$ mode in Figure 8. The amplitude of the backward propagating mode increases as m decreases suggesting it is due to the $O(1/\sqrt{m})$ cross-coupling term in the streaming, however it is always significantly smaller than the $\tilde{a}^+$ mode at the corresponding $(\sqrt{2m}, t)$ point.

In Figures 8(c,d) we show the linear case with no velocity space dissipation, so that the reflection of free energy at the truncation point $a_{N_m} = 0$ generates backwards flux. The backwards flux propagates along $m = -2k^2(t-t_0)^2$ characteristics in both the $\tilde{a}^+$ and $\tilde{a}^-$ modes, but has significantly larger magnitude in the $\tilde{a}^-$ plot. Overall we conclude the decomposition is generally accurate with forwards and backwards modes dominating the $\tilde{a}^+$ and $\tilde{a}^-$ plots respectively.

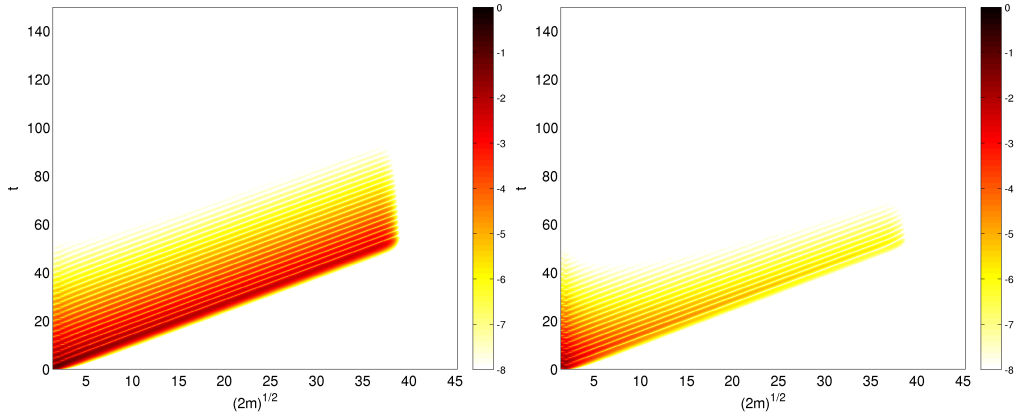

(a) $\log(|\tilde{a}^{+}_{1m}|^2)$, Hou–Li filtering (b) $\log(|\tilde{a}^{-}_{1m}|^2)$, Hou–Li filtering

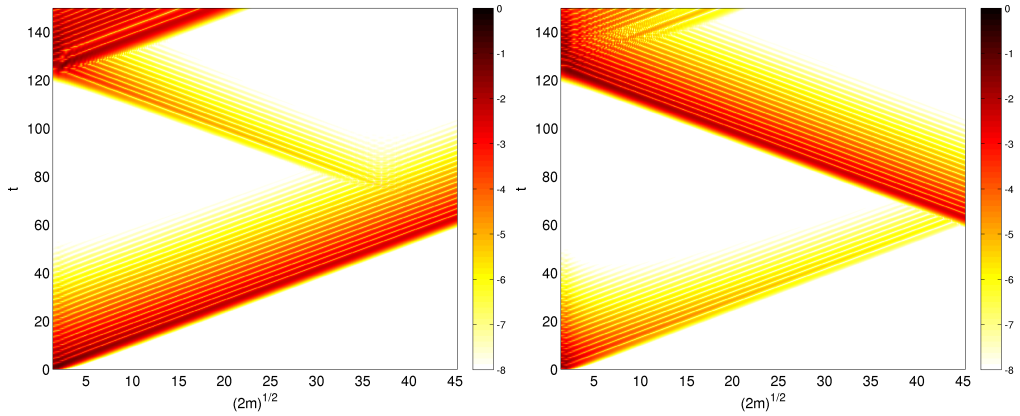

(c) $\log(|\tilde{a}^{+}_{1m}|^2)$, no velocity space dissipation (d) $\log(|\tilde{a}^{-}_{1m}|^2)$, no velocity space dissipation

FIGURE 8. The magnitude of forwards and backwards propagating modes for $k = 0.5$ in the linearized system with and without velocity space dissipation.

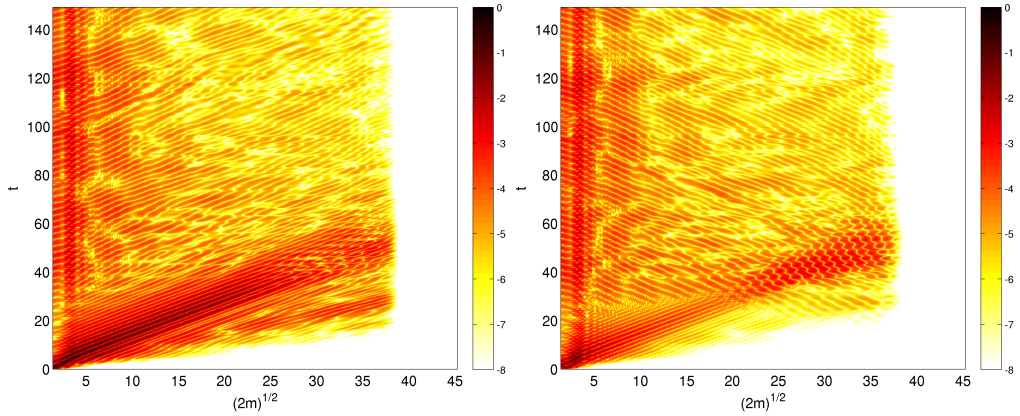

(a) $\log(|\tilde{a}^{+}_{1m}|^2)$ (b) $\log(|\tilde{a}^{-}_{1m}|^2)$

FIGURE 9. The magnitude of forwards and backwards propagating modes for $k = 0.5$ for the nonlinear system.

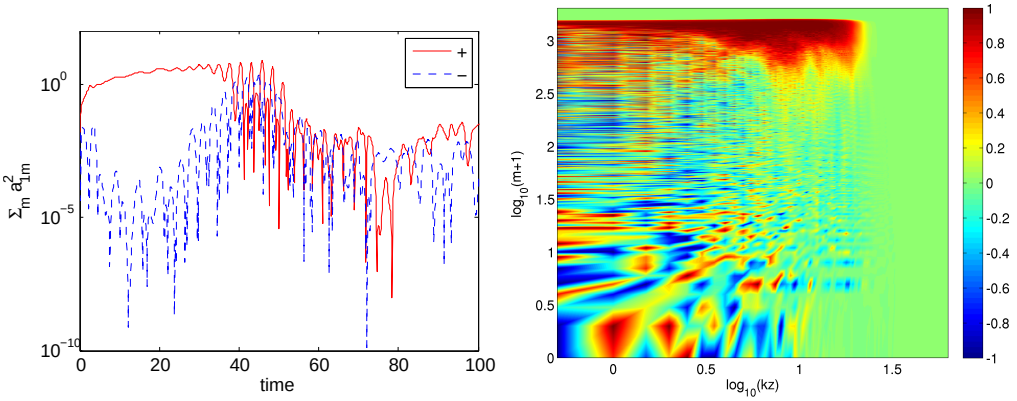

FIGURE 10. Left: contributions to the free energy from forwards and backwards modes, $\sum_m (\tilde{a}^{\pm}_{1m})^2$. Right: time-averaged normalized Hermite flux for the interval $t \in [40, 80]$.

We now plot the corresponding $k = 0.5$ spectra for the nonlinear case in Figure 9. The nonlinear term (4.21) introduces Fourier mode coupling where free energy in other wavenumbers excites both $\tilde{a}^+$ and $\tilde{a}^-$ in the $k = 0.5$ wavenumber. We observe this in Figure 9 where the free energy propagates on the characteristics $m = \pm 2k^2(t - t_0)^2$ respectively. These characteristics appear throughout phase space rather than only near the characteristics that correspond to the propagation of initial conditions, as in Figure 8. This suggests that the $\tilde{a}^-$ modes that cause the increase in the electric field are excited by the nonlinear term. However it remains possible that the back flux is generated by the Boltzmann response or the streaming correction through instabilities that are not excited linearly. To determine which effect is responsible, we plot $\sum_m (\tilde{a}^{\pm}_{1,m})^2$, the contribution to the free energy from the forwards and backwards modes in Figure 10(a). At $t = 20$ when the electric field grows, the contribution to free energy from $\tilde{a}^-$, $\sum_m (\tilde{a}^-_{1m})^2$ grows exponentially. This suggests the increase in free energy is due to a term like $\tilde{a}^-\tilde{a}^-\tilde{a}^+$, such as is found in the nonlinear term contribution to the free energy equation $\tilde{a}^- N^-$.

Turning to the absence of Landau damping at long times, we see from Figure 5 that the free energy contributions reach a steady state where there is very little collisional damping. Moreover from Figure 10(a) we see that the free energy contributions from $\tilde{a}^{\pm}$ balance, showing there is little net flux. This is a statement only about $k = 0.5$, so in Figure 10(b) we plot the normalized Hermite flux (4.17) for all phase space, time-averaged over the interval $t \in [40, 80]$. This shows that indeed there is no systematic Hermite flux towards fine scales. However the growth or decay of the electric field over long timescales, requires a net Hermite flux to persist over long timescales; similarly collisional damping requires a systematic flux to fine scales. Therefore by generating a backward Hermite flux which on average balances with the forward flux, the nonlinearity has effectively suppressed Landau damping.

4.3. *Two stream instability*

We now demonstrate the spectral method for a non-Maxwellian equilibrium f_0 by studying the two-stream instability. This standard problem has been treated in great detail elsewhere (see *e.g.* Grant & Feix (1967); Denavit & Kruer (1971); Cheng & Knorr (1976); Zaki *et al.* (1988); Klimas & Farrell (1994); Nakamura & Yabe (1999); Pohn *et al.* (2005); Heath *et al.* (2012)) and we wish only to illustrate that expected results are obtained with modified SPECTROGK.

We use the new background distribution

$$f_0 = \frac{2v^2}{\sqrt{\pi}} \exp(-v^2), \tag{4.23}$$

and the initial conditions (4.1) with $A = 0.05$, $k = 0.5$ and $L = 4\pi$. The equilibrium is the sum of two Hermite functions

$$f_0 = \sqrt{2}\phi_2(v) + \phi_0(v), \tag{4.24}$$

from which we verify that (2.4) holds. Thus the new equilibrium only enters the Vlasov–Poisson system in the kinetic equation (2.5) as a modification to the response term on the right-hand side,

$$E\frac{\partial f_0}{\partial v} = -\left(2\sqrt{3}\phi_3(v) + \sqrt{2}\phi_1(v)\right) E. \tag{4.25}$$

In Hermite space, this yields an extra source term in the moment equation (3.8),

$$\frac{\partial a_{jm}}{\partial t} + \mathrm{i}k_j \left(\sqrt{\frac{m+1}{2}} a_{j,m+1} + \sqrt{\frac{m}{2}} a_{j,m-1}\right) + \mathsf{N}_{jm} = -\sqrt{2}\hat{E}_j \delta_{m1} - 2\sqrt{3}\hat{E}_j \delta_{m3}, \tag{4.26}$$

with the equations for the electric field (3.9) and (3.10) unchanged.

The bimodal equilibrium (4.23) describes two counter-streaming electron beams, which, with the small initial perturbation, is shown in Figure 11(a). The new source term in (4.26) introduces a linear instability for $k^2 < 2$ (see appendix A). The perturbation is unstable and grows exponentially until the nonlinear term becomes important and saturates the linear growth. In the long time limit, the distribution function approaches the Bernstein–Greene–Kruskal state (Bernstein *et al.* 1957). We see this in our solution, plotted in Figure 11.

5. Conclusion

In this work we have illustrated the usefulness of Fourier–Hermite spectral method for treating the 1+1D Vlasov–Poisson system. The Fourier–Hermite representation presented in section 3 yields an attractive moment-based formulation, which we implemented using a modified version of the SpectroGK gyrokinetics code. The fine velocity space scales which arise due to particle streaming were smoothed using the Hou–Li spectral filter (Hou & Li 2007), which had been successfully applied in physical space in fluid simulations, but had not previously been applied in velocity space. This filtering eliminates recurrence, meaning the method is successful even when phase mixing and filamentation are dominant effects. This is particularly important in regimes like nonlinear Landau damping where the nonlinearity generates structure at fine scales (see Figure 6) which must be distinguishable from recurrence effects.

In section 4 we replicated well-known results for nonlinear Landau damping and the two stream instability, and demonstrated exponential convergence of SpectroGK in both space and velocity space. This benchmarks SpectroGK against solutions obtained by early low-resolution Fourier–Hermite simulations (*e.g.* Armstrong 1967; Grant & Feix 1967), by PIC codes (*e.g.* Denavit & Kruer 1971), by finite element methods (*e.g.* Zaki *et al.* 1988), and by recent discrete Galerkin simulations (Heath *et al.* 2012).

Finally, we studied the flow of free energy in Fourier–Hermite phase space using tools recently developed by Schekochihin *et al.* (2014) for the gyrokinetic equations. We expressed the distribution function as combination of forwards and backwards propagating

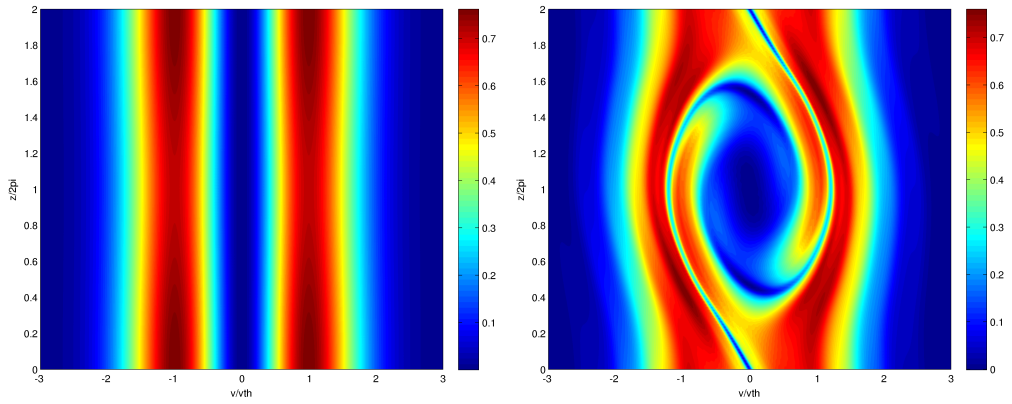

(a) $t = 0$ (b) $t = 20$

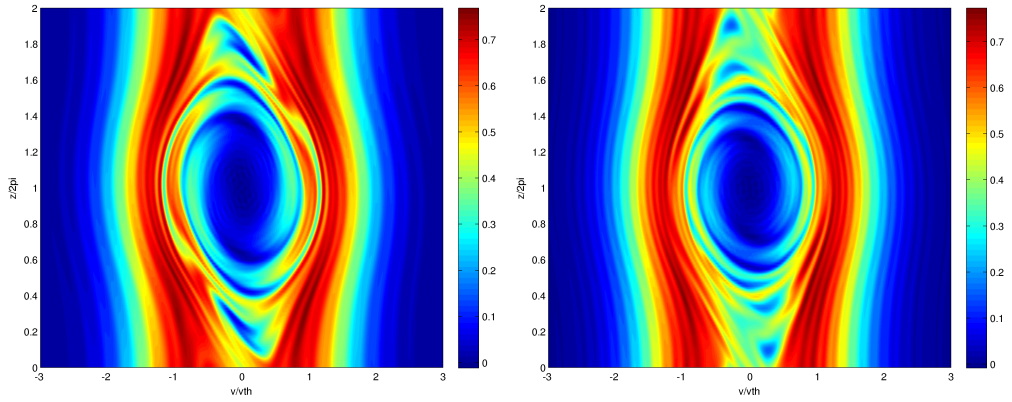

(c) $t = 40$ (d) $t = 60$

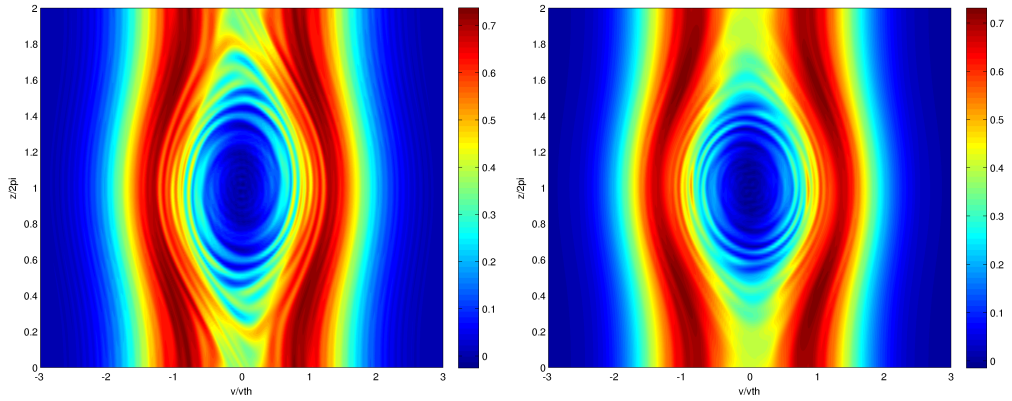

(e) $t = 100$ (f) $t = 160$

FIGURE 11. Time slices of the full distribution function for the two stream instability in (z, v) space, calculated with $(N_k, N_m) = (129, 4096)$ and plotted on the Fourier collocation points and a uniform grid of 4096 point for $v \in [-3, 3]$.

modes in Hermite space, the difference of which represent the flux of free energy. This net Hermite flux is associated with the change in the electric field via the free energy evolution equation (3.18). We showed that the growth in the electric field at $t = 20$ is associated with the generation of backwards propagating modes by the nonlinear term. Both the electric field and the free energy in backwards propagating modes grow exponentially until the free energy content of forwards and backwards propagating modes roughly balance. Thereafter the magnitude of the electric field does not change significantly over time. This is because there is no systematic net flux in Hermite space and therefore no systematic change in the free energy of the electric field. Thus the electric field cannot grow or decay over long times, and so the nonlinearity effectively suppresses Landau damping.

The authors are grateful for fruitful conversations with I. Abel, G. Colyer, S. Cowley, W. Dorland, M. Fox, G. Hammett, E. Highcock, A. Kanekar, G. Plunk, C. Roach, A. Schekochihin, F. van Wyk, and A. Zocco. This work was supported by the UK Engineering and Physical Sciences Research Council through a Doctoral Training Grant award to J.T.P. and an Advanced Research Fellowship [grant number EP/E054625/1] to P.J.D., with additional support from Award No KUK-C1-013-04 made by King Abdullah University of Science and Technology (KAUST). The authors acknowledge the use of the IRIDIS HPC facility through the e-Infrastructure South Centre for Innovation. Some of the results of this research have been achieved using the PRACE-3IP project (FP7 RI-312763) resource FIONN based in Ireland at the DJEI/DES/SFI/HEA Irish Centre for High-End Computing (ICHEC); though access to the HECToR HPC facility [grant number EP/H002081/1]; and through the use of Hartree Centre resources in this work. The STFC Hartree Centre is a research collaboratory in association with IBM providing High Performance Computing platforms funded by the UK's investment in e-Infrastructure. The Centre aims to develop and demonstrate next generation software, optimised to take advantage of the move towards exa-scale computing.

REFERENCES

Abramowitz, M. & Stegun, I. A. 1972 *Handbook of Mathematical Functions: With Formulas, Graphs, and Mathematical Tables*, 10th edn. New York: Dover.

Armstrong, T. P. 1967 Numerical studies of the nonlinear Vlasov equation. *Phys. Fluids* **10** (6), 1269–1280.

Balescu, R. 1963 *Statistical mechanics of charged particles*, , vol. 4. Interscience publishers, New York.

Bardos, C., Golse, F. & Levermore, C. D. 1993 Fluid dynamic limits of kinetic equations II convergence proofs for the Boltzmann equation. *Commun. Pur. Appl. Math.* **46** (5), 667–753.

Bernstein, I. B., Greene, J. M. & Kruskal, M. D. 1957 Exact nonlinear plasma oscillations. *Phys. Rev.* **108** (3), 546.

Birdsall, C. K. & Langdon, A. B. 2004 *Plasma Physics via Computer Simulation*. CRC Press.

Bouchut, F. 1993 Existence and uniqueness of a global smooth solution for the Vlasov–Poisson–Fokker–Planck system in three dimensions. *J. Func. Anal.* **111**, 239–258.

Boyd, J. P. 2001 *Chebyshev and Fourier Spectral Methods*. *Dover books on mathematics*. New York: Dover.

Burnett, D. 1935 The distribution of velocities in a slightly non-uniform gas. *Proc. Lond. Math. Soc.* **s2-39** (1), 385–430.

Burnett, D. 1936 The distribution of molecular velocities and the mean motion in a non-uniform gas. *Proc. Lond. Math. Soc.* **s2-40** (1), 382–435.

Case, K. M. 1959 Plasma oscillations. *Ann. Phys.-New York* **7** (3), 349–364.

Cheng, C. Z. & Knorr, G. 1976 The integration of the Vlasov equation in configuration space. *J. Comput. Phys.* **22** (3), 330–351.

Dawson, J. M. 1983 Particle simulation of plasmas. *Rev. Mod. Phys.* **55**, 403–447.

Denavit, J. & Kruer, W. L. 1971 Comparison of numerical solutions of the Vlasov equation with particle simulations of collisionless plasmas. *Phys. Fluids* **14**, 1782–1791.

Dolbeault, J. 1999 Free energy and solutions of the Vlasov–Poisson–Fokker–Planck system: external potential and confinement (Large time behavior and steady states). *J. Math. Pures Appl.* **78**, 121–157.

Dorland, W., Highcock, E. G., Barnes, M., Hammett, G. W., Numata, R., Tatsuno, T., Roach, C., Colyer, G., Baumgaertel, J. & Dickinson, D. 2009 Gyrokinetic simulations project. See http://gyrokinetics.sourceforge.net/.

Durran, D. R. 1991 The third-order Adams-Bashforth method: an attractive alternative to leapfrog time-differencing. *Mon. Weather Rev.* **119**, 702–720.

Durran, D. R. 1999 *Numerical Methods for Wave Equations in Geophysical Fluid Dynamics*. Springer.

Fahey, M. R. & Candy, J. 2004 Gyro: A 5-D gyrokinetic-Maxwell solver. In *Proceedings of the 2004 ACM/IEEE conference on Supercomputing*, pp. 26–. Washington, DC, USA: IEEE Computer Society.

Filbet, F., Sonnendrücker, E. & Bertrand, P. 2001 Conservative numerical schemes for the Vlasov equation. *J. Comput. Phys.* **172** (1), 166–187.

Fried, B.D. & Conte, S.D. 1961 *The Plasma Dispersion Function: The Hilbert Transform of the Gaussian*. Academic Press.

Frigo, M. & Johnson, S. G. 2005 The design and implementation of FFTW3 **93** (2), 216–231.

Glassey, Robert T. 1996 *The Cauchy Problem in Kinetic Theory*. Philadelphia: Society for Industrial and Applied Mathematics.

Golse, F. & Saint-Raymond, L. 2004 The Navier–Stokes limit of the Boltzmann equation for bounded collision kernels. *Inventiones Mathematicae* **155**, 81–161.

Grad, H. 1949*a* Note on N-dimensional Hermite polynomials. *Commun. Pur. Appl. Math.* **2** (4), 325–330.

Grad, H. 1949*b* On the kinetic theory of rarefied gases. *Commun. Pur. Appl. Math.* **2** (4), 331–407.

Grad, H. 1958 Principles of the kinetic theory of gases. In *Thermodynamik der Gase* (ed. S. Flügge), *Handbuch der Physik*, vol. 12, pp. 205–294. Berlin: Springer-Verlag.

Grant, F. C. & Feix, M. R. 1967 Fourier–Hermite solutions of the Vlasov equations in the linearized limit. *Phys. Fluids* **10** (4), 696–702.

Hallatschek, K. 2004 Thermodynamic potential in local turbulence simulations. *Phys. Rev. Lett.* **93**, 125001.

Hammett, G. W., Beer, M. A., Dorland, W., Cowley, S. C. & Smith, S. A. 1993 Developments in the gyrofluid approach to tokamak turbulence simulations. *Plasma Phys. Control. Fusion* **35** (8), 973.

Hatch, D. R., Jenko, F., Bañón Navarro, A. & Bratanov, V. 2013 Transition between saturation regimes of gyrokinetic turbulence. *Phys. Rev. Lett.* **111**, 175001.

Heath, R. E., Gamba, I. M., Morrison, P. J. & Michler, C. 2012 A discontinuous Galerkin method for the Vlasov–Poisson system. *J. Comput. Phys.* **231** (4), 1140–1174.

Highcock, E. G., Barnes, M., Parra, F. I., Schekochihin, A. A., Roach, C. M. & Cowley, S. C. 2011 Transport bifurcation induced by sheared toroidal flow in tokamak plasmas. *Phys. Plasmas* **18**, 102304.

Hockney, R. W. & Eastwood, J. W. 1988 *Computer simulation using particles*. CRC Press.

Hou, T. Y. & Li, R. 2007 Computing nearly singular solutions using pseudo-spectral methods. *J. Comput. Phys.* **226** (1), 379–397.

Howes, G. G., Cowley, S. C., Dorland, W., Hammett, G. W., Quataert, E. & Schekochihin, A. A. 2006 Astrophysical Gyrokinetics: Basic Equations and Linear Theory. *Astrophys. J. Suppl.* **651**, 590–614.

Jenko, F., Dorland, W., Kotschenreuther, M. & Rogers, B. N. 2000 Electron temperature gradient driven turbulence. *Phys. Plasmas* **7** (5), 1904–1910.

Joyce, G., Knorr, G. & Meier, H. K. 1971 Numerical integration methods of the Vlasov equation. *J. Comput. Phys.* **8** (1), 53–63.

Kanekar, A., Schekochihin, A. A., Dorland, W. & Loureiro, N. F. 2014 Fluctuation-dissipation theorems for a plasma-kinetic Langevin equation. ArXiv:1403.6257.

Klimas, A. J. & Farrell, W. M. 1994 A splitting algorithm for Vlasov simulation with filamentation filtration. *J. Comput. Phys.* **110** (1), 150–163.

Krommes, J. A. 2012 The gyrokinetic description of microturbulence in magnetized plasmas. *Annu. Rev. Fluid Mech.* **44**, 175–201.

Krommes, J. A. & Hu, G. 1994 The role of dissipation in the theory and simulations of homogeneous plasma turbulence, and resolution of the entropy paradox. *Phys. Plasmas* **1**, 3211–3238.

Landau, L. D. 1946 On the vibrations of the electronic plasma. *J. Phys.-U.S.S.R.* **10** (25).

Lénard, A. & Bernstein, I. B. 1958 Plasma oscillations with diffusion in velocity space. *Phys. Rev.* **112** (5), 1456–1459.

Lifshitz, E. M. & Pitaevskii, L. P. 1981 *Physical kinetics*. Pergamon press, Oxford, translated from Russian by J. B. Sykes and R. N. Franklin.

Lions, P.-L. & Masmoudi, N. 2001 From the Boltzmann equations to the equations of incompressible fluid mechanics, I. *Arch. Ration. Mech. An.* **158**, 173–193.

Loureiro, N. F., Schekochihin, A. A. & Zocco, A. 2013 Fast collisionless reconnection and electron heating in strongly magnetized plasmas. *Phys. Rev. Lett.* **111** (2), 025002.

Nakamura, T. & Yabe, T. 1999 Cubic interpolated propagation scheme for solving the hyper-dimensional Vlasov–Poisson equation in phase space. *Comput. Phys. Commun.* **120** (2-3), 122–154.

Ng, C. S., Bhattacharjee, A. & Skiff, F. 1999 Kinetic eigenmodes and discrete spectrum of plasma oscillations in a weakly collisional plasma. *PRL* **83** (10), 1974–1977.

Ng, C. S., Bhattacharjee, A. & Skiff, F. 2004 Complete spectrum of kinetic eigenmodes for plasma oscillations in a weakly collisional plasma. *Phys. Rev. Lett.* **92** (6), 065002.

Ng, C. S., Bhattacharjee, A. & Skiff, F. 2006 Weakly collisional Landau damping and three-dimensional Bernstein–Greene–Kruskal modes: New results on old problems. *Phys. Plasmas* **13** (5), 055903.

Orszag, S. A. 1971 On the elimination of aliasing in finite-difference schemes by filtering high-wavenumber components. *J. Atmos. Sci.* **28** (6), 1074–1074.

Parker, J. T. & Dellar, P. J. 2014 Hermite expansions with hypercollisionality for velocity space degrees of freedom in ion-temperature-gradient driven instabilities. In preparation.

Parker, J. T., Highcock, E. G. & J., Dellar P. 2014 SpectroGK: a fully spectral astrophysical gyrokinetics code. In preparation.

Parker, S. E. & Carati, D. 1995 Renormalized dissipation in plasmas with finite collisionality. *Phys. Rev. Lett.* **75** (3), 441–444.

Pauli, W. 2000 *Statistical Mechanics*. Dover Publications.

Peeters, A. G., Camenen, Y., Casson, F. J., Hornsby, W. A., Snodin, A. P., Strintzi, D. & Szepesi, G. 2009 The nonlinear gyro-kinetic flux tube code GKW. *Comput. Phys. Commun.* **180** (12), 2650–2672.

Plunk, G. G. & Parker, J. T. 2014 Irreversible energy flow in forced Vlasov dynamics. ArXiv:1402.7230.

Pohn, E., Shoucri, M. & Kamelander, G. 2005 Eulerian Vlasov codes. *Comput. Phys. Commun.* **166** (2), 81–93.

Schekochihin, A. A., Kanekar, A., Hammett, G. W., Dorland, W. & Loureiro, N. F. 2014 Stochastic advection and phase mixing in a collisionless plasma. In preparation.

Van Kampen, N. G. 1955 On the theory of stationary waves in plasmas. *Physica* **21**, 949–963.

Zaki, S. I., Boyd, T. J. M. & Gardner, L. R. T. 1988 A finite element code for the simulation of one-dimensional Vlasov plasmas. II. applications. *J. Comput. Phys.* **79** (1), 200–208.

Zhou, T., Guo, Y. & Shu, C.-W. 2001 Numerical study on Landau damping. *Physica D* **157** (4), 322–333.

Zocco, A. & Schekochihin, A. A. 2011 Reduced fluid-kinetic equations for low-frequency dynamics, magnetic reconnection, and electron heating in low-beta plasmas. *Phys. Plasmas* **18** (10), 102309.

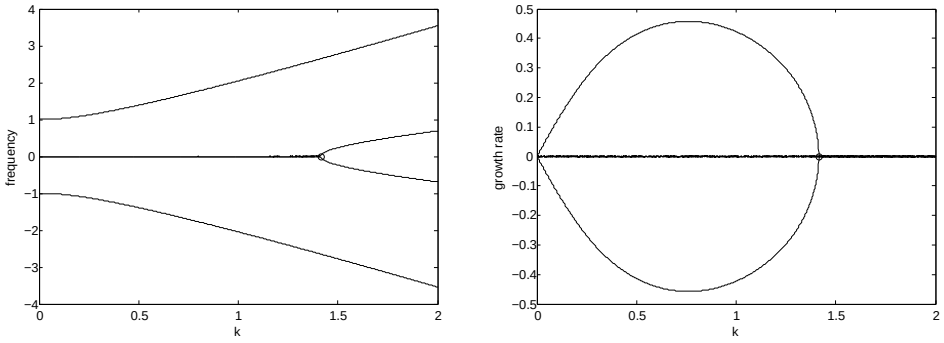

FIGURE 12. Dispersion relation for the two stream instability: frequency (left) and growth rate (right) against wavenumber k. The small circle on the k-axis marks the wavenumber $k = \sqrt{2}$.

Appendix A. Linear dispersion relation

To illustrate the appearance of a linear instability for the non-Maxwellian equilibrium (4.23), we derive the linear dispersion relation based on the first four Hermite moments in (3.8) and (4.26). This may be viewed as a simple collisionless fluid model. This does not capture decay rates, but is sufficient to determine regions of linear instability.

The linear equation is parameterized by k, so we solve for time eigenfunctions of the form $a_m(k,t) = \bar{a}_m(k)\mathrm{e}^{-i\omega t}$. The first four moments are

$$\begin{pmatrix} -\mathrm{i}\omega & \mathrm{i}k & 0 & 0 \\ \mathrm{i}\left(\frac{k}{\sqrt{2}} + \frac{\sqrt{2}}{k}\right) & -\mathrm{i}\omega & \mathrm{i}k & 0 \\ 0 & \mathrm{i}k & -\mathrm{i}\omega & \mathrm{i}k\sqrt{3/2} \\ \mathrm{i}\beta 2\sqrt{3}/k & 0 & \mathrm{i}k\sqrt{3/2} & -\mathrm{i}\omega \end{pmatrix} \begin{pmatrix} a_0 \\ a_1 \\ a_2 \\ a_3 \end{pmatrix} = 0, \tag{A 1}$$

where $\beta = 0$ for the nonlinear Landau-damping problem, and $\beta = 1$ for the two stream instability. This yields the dispersion relation

$$\omega^4 - (3k^2+1)\omega^2 + \frac{3k^2}{4}\left(k^2 + 2 - 4\beta\right) = 0, \tag{A 2}$$

with solutions

$$\omega^2 = \frac{1}{2}\left[(3k^2+1) \pm \sqrt{(3k^2+1)^2 - 3k^2(k^2+2-4\beta)}\right]. \tag{A 3}$$

The plasma is stable if ω^2 is real and non-negative, that is if

$$(3k^2+1)^2 \geqslant (3k^2+1)^2 - 3k^2\left(k^2+2-4\beta\right). \tag{A 4}$$

For nonlinear Landau-damping ($\beta = 0$) this is always true and all modes are linearly stable. For the two stream instability ($\beta = 1$), modes corresponding to the $+$ sign in (A 3) are stable, while modes corresponding to the $-$ sign are unstable for wavenumbers $0 < k < \sqrt{2}$. The dispersion relation for the two stream instability is shown in Figure 12.